Quaternary Research 86 (2016) 13–33

Contents lists available at ScienceDirect

Quaternary Research

journal homepage: http://www.journals.elsevier.com/quaternary-research

A regional record of expanded Holocene wetlands and prehistoric human occupation from paleowetland deposits of the western Yarlung Tsangpo valley, southern Tibetan Plateau

Adam M. Hudson [a, *], John W. Olsen [b], Jay Quade [a], Guoliang Lei [c], Tyler E. Huth [d], Hucai Zhang [e]

[a] Department of Geosciences, University of Arizona, Tucson, AZ, 85721, USA
[b] School of Anthropology, University of Arizona, Tucson, AZ, 85721, USA
[c] College of Geographical Sciences, Fujian Normal University, Fujian, 350007, China
[d] Department of Geology and Geophysics, University of Utah, Salt Lake City, UT, USA
[e] College of Tourism and Geography, Yunnan Normal University, Kunming, 650500, China

ARTICLE INFO

Article history:
Received 30 October 2015
Available online 20 May 2016

Keywords:
Radiocarbon
Black mat
Wetland
Microlithic archaeology
Indian Summer Monsoon
Holocene
Tibetan Plateau

ABSTRACT

The Asian Monsoon, which brings ~80% of annual precipitation to much of the Tibetan Plateau, provides runoff to major rivers across the Asian continent. Paleoclimate records indicate summer insolation and North Atlantic paleotemperature changes forced variations in monsoon rainfall through the Holocene, resulting in hydrologic and ecologic changes in plateau watersheds. We present a record of Holocene hydrologic variability in the Yarlung Tsangpo (YT) valley of the southern Tibetan Plateau, based on sedimentology and ^{14}C dating of organic-rich 'black mats' in paleowetlands deposits, that shows changes in wetlands extent in response to changing monsoon intensity. Four sedimentary units indicate decreasing monsoon intensity since 10.4 ka BP. Wet conditions occurred at ~10.4 ka BP, ~9.6 ka BP and ~7.9–4.8 ka BP, with similar-to-modern conditions from ~4.6–2.0 ka BP, and drier-than-modern conditions from ~2.0 ka BP to present. Wetland changes correlate with monsoon intensity changes identified in nearby records, with weak monsoon intervals corresponding to desiccation and erosion of wetlands. Dating of *in situ* ceramic and microlithic artifacts within the wetlands indicates Epipaleolithic human occupation of the YT valley after 6.6 ka BP, supporting evidence for widespread colonization of the Tibetan Plateau in the early and mid-Holocene during warm, wet post-glacial conditions.

© 2016 University of Washington. Published by Elsevier Inc. All rights reserved.

Introduction

The Tibetan Plateau is the highest contiguous landmass on Earth, forming a climatological and biogeographic barrier dividing the Indian subcontinent from arid Central Asia. The majority of the plateau is characterized by a cold, arid environment, but it holds the headwaters of many major rivers that provide water to the surrounding Asian continent (e.g. Yellow River, Ganges-Brahmaputra, Indus River). These rivers are fed by seasonal precipitation from the Asian Summer Monsoon and winter Westerly storms combined with melt runoff derived from numerous alpine glaciers. The importance of plateau watersheds for water resources has generated great interest in the paleoclimate history and climatic controls on hydrologic variability of the Tibetan Plateau.

Variations in climate over the course of the Holocene, dominated by the changing intensity of the summer monsoon, have resulted in significant hydrologic changes across the plateau region. Monsoon intensity on the Tibetan Plateau has mainly been reconstructed using hydrologic indicators in an array of proxies preserved in lake cores (Van Campo and Gasse, 1993; Demske et al., 2009; Mügler et al., 2010; Li et al., 2011; An et al., 2012; Leipe et al., 2014), lake shorelines (Kong et al., 2007; Lee et al., 2009; Wünnemann et al., 2010, 2015; Pan et al., 2012; Hudson et al., 2015; Huth et al., 2015; Ahlborn et al., 2016), ice cores (Thompson et al., 1997; Liu et al., 1998), and speleothems (Cai et al., 2012). In general, paleoclimate records indicate wetter-than-modern conditions during the early to mid-Holocene, approximately 11.0–4.0 ka BP, with more intensification relative

* Corresponding author.
E-mail address: amhudson@email.arizona.edu (A.M. Hudson).

http://dx.doi.org/10.1016/j.yqres.2016.04.001
0033-5894/© 2016 University of Washington. Published by Elsevier Inc. All rights reserved.

https://doi.org/10.1016/j.yqres.2016.04.001 Published online by Cambridge University Press

to modern over the western Tibetan Plateau (Hudson and Quade, 2013; Liu et al., 2013). However, the inferred wettest period of the Holocene may vary depending upon location, and is likely obscured by age uncertainties (Li et al., 2011; Hou et al., 2012). Additional well-dated records are required to provide a clear picture of the regional variability in timing of wet periods during the Holocene.

The Yarlung Tsangpo (YT; tsangpo = river), which runs west to east across the southernmost area of the Tibetan Plateau, is one of the major watersheds providing runoff to the Brahmaputra River in northeastern India. It drains a large portion of the high Himalayan and Gangdise Shan mountain ranges, and flows for more than 1500 km at high elevation, incorporating runoff from drainages across the entirety of the southern plateau (Fig. 1A). Modern wetlands and paleowetland deposits are found commonly along the margins of the low-gradient reaches of the YT, supported by local spring discharge and shallow local water tables. Sediments deposited in these wetlands are potential archives of past hydrologic conditions, reflecting changes in vegetation cover, spring discharge, and water table elevation in response to changing precipitation (Quade et al., 1998, 2008; Betancourt et al., 2000; Rech et al., 2003; Pigati et al., 2014; Springer et al., 2015).

Paleowetlands also commonly host the archaeological remains of prehistoric people, particularly in desert regions (Ashley et al., 2009). *In situ* artifacts within these deposits provide critical chronological control on site occupation that is often lacking in open-air sites. Stone and ceramic artifacts in surface and stratified archaeological sites are widespread on the Tibetan Plateau in sediments dating to the early and mid-Holocene, coeval with warm and wet climate conditions (Brantingham et al., 2001, 2007; 2013; Aldenderfer and Zhang, 2004). However, few archaeological sites of early/mid-Holocene age are securely dated radiometrically, and additional work is required to understand the timing and extent of plateau colonization by prehistoric peoples. We present a ^{14}C-dated record of wetlands formation in the upper YT valley that provides a new perspective on Holocene hydrologic changes in the southern Tibetan Plateau. In addition to reconstructing paleohydrology and climate, we build on previous work (Hudson et al., 2014) constraining the age and history of prehistoric human occupation in the YT valley using the paleowetlands record.

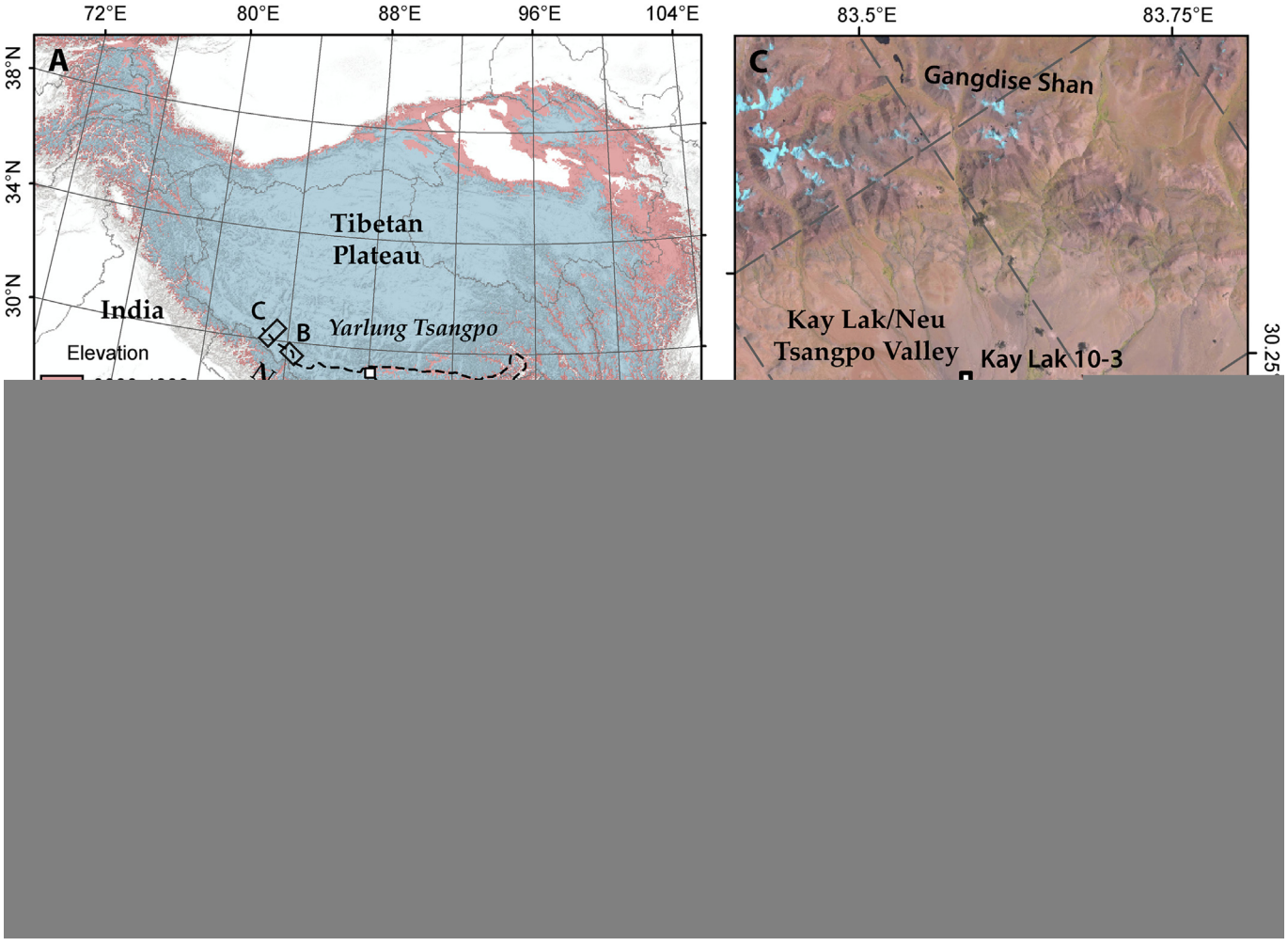

Figure 1. Study locality maps, Yarlung Tsangpo valley. Major rivers (e.g. Yarlung Tsangpo) are labeled in italics. Study localities are shown by white squares, modern settlements by white circles. A – Tibetan Plateau region, map areas of B and C shown. Base map hillshade based on NASA SRTM 90 m DEM. Land area between 3000 and 4000 m asl and >4000 m asl shown in pink and blue shading, respectively. B – Zhongba valley and locality. Map area of Fig. 3 shown by black box. C – Kay Lak valley, Yulai Cun and Tsangpo 18 localities; ice and snow in blue, vegetation in green. Panel B and C base images are Landsat 5 Thematic Mapper true color satellite images from November 4, 2011 and September 18, 2009, respectively (available online at http://earthexplorer.usgs.gov/). (For interpretation of the references to colour in this figure legend, the reader is referred to the web version of this article.)

https://doi.org/10.1016/j.yqres.2016.04.001 Published online by Cambridge University Press

Upper Yarlung Tsangpo Valley study area

Our study area covers a large part of the southwestern Tibetan Plateau in the headwaters of the YT (Fig. 1). Valley bottoms are near 4600 m above sea level (asl), rising to peaks >6000 m asl. Geologically, the study area is located in the Indus-Yarlung suture zone, where local bedrock geology is highly variable. It is dominated by Cretaceous sedimentary mélange of the Xigaze forearc in the bottoms of the YT and Kay Lak valleys. The headwaters of the Kay Lak valley are made up of sedimentary rocks of the Miocene Kailas Formation and volcanic and plutonic rocks associated with the Cretaceous-Eocene Gangdise volcanic arc (Ding et al., 2005; Styron et al., 2013; Carrapa et al., 2015).

Modern seasonal temperature in the valley bottoms ranges from −12°C in January to 12°C in June, and averages 0°C annually. Modern precipitation, based on Tropical Rainfall Measuring Mission (TRMM) gridded data 1998–2010 is ~250 mm/yr in the western YT valley (Kummerow et al., 1998), increasing to ~400 mm/yr at Ngamring, proximal to the easternmost study locality. Approximately 80% of precipitation falls during summer and fall (May–October), derived from southwesterly Indian Summer Monsoon storms (Tian et al., 2007; Bookhagen and Burbank, 2010). The remaining precipitation comes from winter Westerly storms, which bring a larger proportion (up to 50%) of annual precipitation to the western part of the Tibetan Plateau and northwestern Himalaya, outside the study area. River runoff in Himalayan catchments directly adjacent to the study area shows similar seasonality to rainfall, peaking during the monsoon season, and with summer and fall rainfall (May–October) ultimately contributing >70% of annual runoff (Bookhagen and Burbank, 2010). Within these same catchments a significant part of the groundwater-supported baseflow during the winter season is derived from prior summer precipitation, and water table elevation peaks during the summer season, suggesting shallow groundwater conditions also respond dominantly to summer rainfall conditions (Andermann et al., 2012).

Because of the cold, arid climate, vegetation is limited to grasses and small shrubs (Yu et al., 2001), with plant biomass growing preferentially at lower elevation adjacent to stream channels, spring discharge outlets, and in wetlands (Fig. 2A, B). Modern permanent settlements like Zhongba, Paryang and Yulai Cun (Fig. 1B, C), and camps of nomadic herding groups tend to be focused in these locations due to the availability of water. This type of high productivity water-marginal environment forms the modern analog for deposition of the organic-rich 'black mat' horizons used for ^{14}C dating in the sediment sequences studied here (Fig. 2C, D). The term 'black mat' refers to distinct, semi-continuous beds of organic-rich sediment associated with deposition in past wetlands environments (Quade et al., 1998; Haynes, 2008). The organic matter in these horizons is typically of terrestrial plant origin (Harris-Parks, 2016), likely forming syn- or post-depositional to the

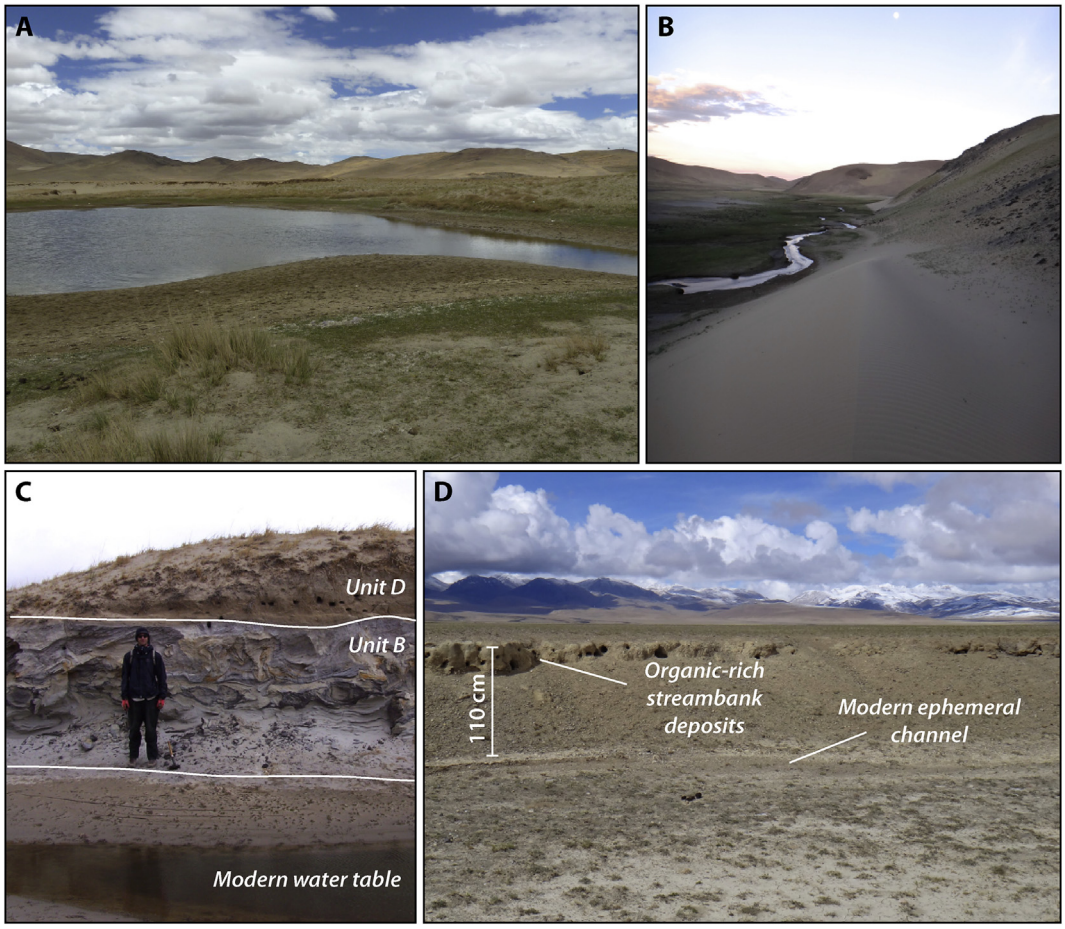

Figure 2. Modern analog environments and corresponding paleowetlands deposits in the upper Yarlung Tsangpo valley. A – interdune pond and surrounding vegetation, Zhongba locality. Photo credit: A. Hudson, June 16, 2010. B – stream channel with concentrated vegetation along the margins, Zhongba locality. Photo credit: A. Hudson, June 22, 2013. C – example of organic-rich 'black mat' paleowetlands deposits (Unit B) overlain by eolian deposits (Unit D) above the modern interdune pond water level, Zhongba locality. Geologist for scale is 1.9 m height. Photo credit: J. Quade, June 17, 2010. D – example of perched streambank paleowetlands deposits above the now ephemeral stream channel, Kay Lak locality. Streambank deposits are 110 cm above the stream channel. Photo credit: A. Hudson, June 11, 2011.

https://doi.org/10.1016/j.yqres.2016.04.001 Published online by Cambridge University Press

sediment by decay of emergent plants and their roots growing on the banks or in shallow water regions of paleowetlands streams and ponds.

We consider five paleowetlands localities located at valley bottom elevations in this study (4600–4700 m asl). Two have been previously reported (Hudson et al., 2014) and three are new in this work. With the exception of the easternmost locality, Tsangpo 20, they are north of the modern river course of the YT. The four western localities are separated by a maximum of 100 km, both within the main valley (Yulai Cun, Tsangpo 18, Zhongba), and in the Kay Lak valley surrounding the YT tributary river, the Neu Tsangpo (Kay Lak valley group sites 10-3, 13-1, 13-3; Fig. 1C). Tsangpo 20 is located south of the main river in a tributary valley east of the modern town of Ngamring (Fig. 1B). The deposits at all sites consist of similar sedimentary facies, but those in the main YT valley are paleowetlands inundating dunes, whereas those in the Kay Lak valley are located along the channel margins and floodplains of small tributary streams of the Neu Tsangpo.

Interdune wetlands sites: Zhongba, Yulai Cun, Tsangpo 18, Tsangpo 20

Within the study area, the YT forms an extensive braided river system with a low gradient and high sediment load fed by the numerous alpine glaciers in the surrounding Himalaya and Gangdise Shan mountain ranges (Fig. 1). Sand from this system is reworked into large fields of parabolic and barchan dunes, mostly on the north side of the main valley downwind under the prevailing southwesterly circulation pattern (Tian et al., 2007). In many locations systems of wet meadows, marshes, and shallow ponds, generally totaling 10's of km^2 in area, form on the lower valley slopes where the shallow water table intersects blown-out depressions between dunes (Fig. 2A). These interdune wetlands support abundant terrestrial grasses on their margins, aquatic plants within individual pools, and abundant aquatic (genus *Radix*, *Gyraulus*, *Pisidium*), semi-aquatic (Succineidae) and terrestrial (Puppillidae) mollusks.

Four study localities are located in extant interdune wetlands systems. Zhongba (Figs. 1B and 3), covers approximately 1 km^2 of wetlands near the settlement of the same name, consisting of multiple ponds ringed by paleowetlands deposits, located on a southwest facing hillslope at elevations between 4565 and 4580 m asl. Tsangpo 18 consists of two outcrops of paleowetlands sediments approximately 65 m apart on the east side of an interdune pond near the settlement of Paryang (Fig. 1C). Zhongba and Tsangpo 18 have been previously studied (Hudson et al., 2014), but are supplemented with additional sedimentary descriptions and new ^{14}C ages presented here. Yulai Cun is located 18 km northwest of Tsangpo 18 (Fig. 1C), and consists of two outcrops of paleowetlands sediments surrounding a single pond. Tsangpo 20 is located in a small set of wetlands within an active alluvial drainage where Holocene erosion has exposed paleowetlands horizons in the walls of ephemeral streamcuts. At all sites, the modern interdune wet meadow and pond environments are ringed by extensive organic and carbonate-rich deposits exposed up to 3 m above the current water table elevation (Fig. 2C). In general these deposits are composed of well-sorted dune sand overprinted by orange Fe-staining, gray 'black mat' horizons, and interbedded with silty, calcareous marsh marls. Bedding within these deposits ranges from gently undulating to highly contorted, due to extensive soft-sediment deformation. Fossil *Radix* sp. and *Pisidium* sp. mollusk shells are common, and *in situ* lithic and ceramic artifacts are occasionally found. Collections

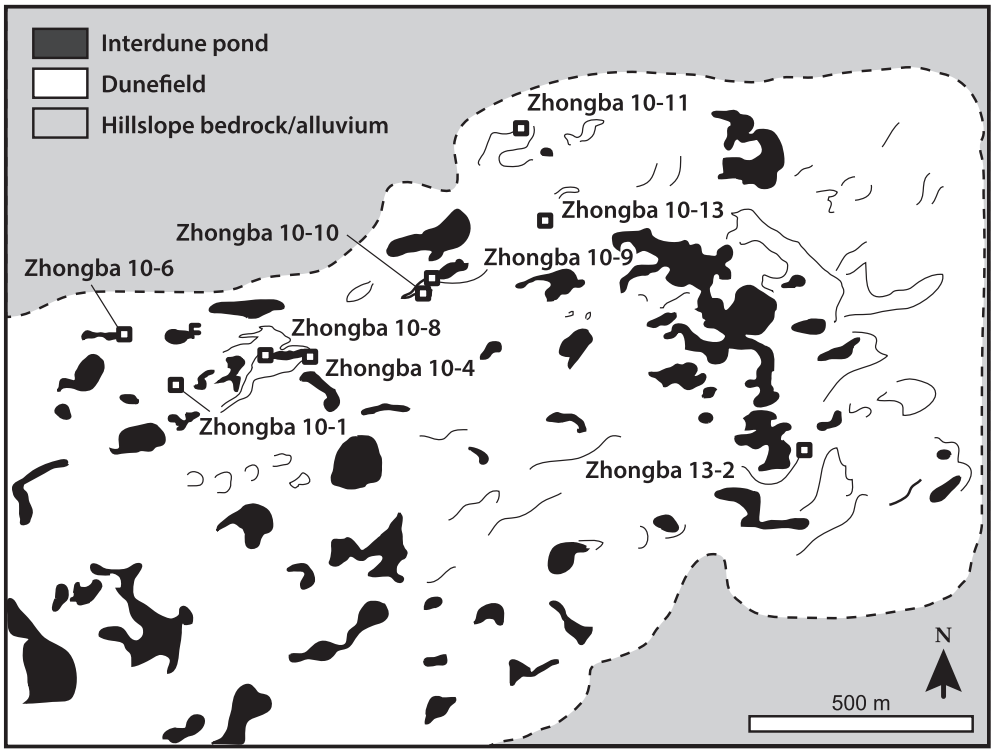

Figure 3. Schematic map of the Zhongba interdune wetlands locality. Approximate edge of dunefield shown by dashed line. Approximate footprint of Fig. 3 is shown in Fig. 1B. Locations of individual stratigraphic sections are shown by open squares. Current pond extents are shaded black, the current dunefield in white, and surrounding hillslope bedrock and alluvium in gray.

https://doi.org/10.1016/j.yqres.2016.04.001 Published online by Cambridge University Press

of artifacts are also found on the eroding surface horizons of paleowetlands deposits.

Kay Lak valley sites: Kay Lak 10-3, 13-1, and 13-3

The drainage basin of the Kay Lak valley is bounded by the Gangdise Shan to the north, and is separated from the main YT valley by a range of hills to the south (Fig. 1C). The valley floor contains many southward-directed tributary stream channels originating in the glaciated valleys of the Gangdise Shan, which feed the Neu Tsangpo in the valley center. Organic-rich wet meadows parallel the modern river channel and its perennial tributaries, while vegetation-poor alluvium overlain by eolian sand dominates the interfluves (Fig. 2B, D). Remnants of ephemeral channels are clearly visible on the alluvial fans deposited on the sides of the valley.

Three study sites are grouped within the Kay Lak valley: two in the open main valley north of the Neu Tsangpo (Kay Lak 10-3, 13-1), and one along the westernmost ephemeral tributary channel (Kay Lak 13-3). Sediments in the main valley sites consist of black mats and marls similar to those observed in the interdune wetland sites. Sediments along the Neu Tsangpo tributary consist of coarse alluvium interbedded with black mat horizons. Kay Lak 10-3 and 13-3 are associated with *in situ* and surface collections of artifacts, respectively.

Methods

Site identification and sampling methods

Sites were identified by targeting modern wetlands on satellite imagery and by field reconnaissance. In the field, sedimentary sequences were described and measured in exposed stratigraphic sections in the sides of the interdune depressions or alluvial streamcuts at each locality. *In situ* plant macrofossil, black mat, and mollusk shell ^{14}C samples were collected from most study sections (Table 1). Additional artifacts and ^{14}C samples from wetlands deposits exposed *in situ* at the modern surface were collected where vertical exposures were not available. At sites where artifacts were already exposed *in situ* or uncovered in the process of recording profiles, they were described and left in place. Collections of artifacts and *débitage* in lag deposits on the surfaces surrounding the sites were made throughout the wetlands.

Dating methods

All samples used for ^{14}C dating were initially dried overnight in a 70°C drying oven at the University of Arizona. Mollusk shell samples were rinsed ultrasonically, submerged in H_2O_2 for 4 h to remove organic matter, and dried prior to acid dissolution. Organic ^{14}C samples consisting of well-preserved plant macrofossils were subjected to a standard acid-base-acid (ABA) treatment with 6 N HCl and 2% NaOH, and the NaOH-insoluble humin residue fraction (hereafter residue) was retained for combustion. The black mats in the wetlands deposits are made up of bulk organic matter that is fine grained and mixed with modern roots dispersed within the sediments. Therefore, bulk organic samples were subjected to a modified pretreatment procedure. Prior to ABA treatment, sediments were disaggregated in distilled water and shaken vigorously to free modern roots, which were then floated overnight and decanted. The standard ABA treatment was then applied, but the NaOH-soluble humic acid fraction (hereafter humates) was precipitated from the 2% NaOH solution using 6 N HCl, dried overnight, and also retained for combustion. Thirteen samples were dated using both the bulk sediment residue and humate fractions to assess the potential age offset introduced by dating different fractions.

Organic samples were combusted under vacuum at 900°C with CuO powder and Ag foil. Mollusk shell samples were dissolved under vacuum using 100% H_3PO_4. The produced CO_2 gas was extracted under vacuum, cryogenically purified, and passed through a 600°C Cu/Ag furnace to remove contaminant gases. Purified CO_2 samples were then graphitized using Zn and Fe powder following Slota et al. (1987). $\delta^{13}C$ and AMS ^{14}C measurements were conducted at the Arizona AMS Laboratory. Raw ^{14}C ages were calibrated and probability density functions for individual ages were produced using the OxCal 4.2 software with the IntCal13 calibration curve (Bronk Ramsey, 2009; Reimer et al., 2013). All calibrated ^{14}C ages are reported as the median age of the calendar range plus or minus 2σ error.

Optically stimulated luminescence (OSL) dating of two ceramic sherds was performed by the Luminescence Laboratory at the University of Washington. Prior to measurement, each sherd was broken to expose a fresh profile. Material was drilled from the center of the cross-section, more than 2 mm from either surface, using a tungsten carbide drill tip, and then ground gently by an agate mortar and pestle, treated with HCl to remove carbonate, and then settled in acetone for 2–20 min to separate the 1–8 μm fraction.

Optically stimulated luminescence (OSL) and infrared stimulated luminescence (IRSL) were carried out on five separate aliquots of this fraction for each sample following procedures adapted from Banerjee et al. (2001) and Roberts and Wintle (2001) on a Risø TL-DA-15 automated reader by a succession of two stimulations: first, 100 s at 60°C of IRSL (880 nm diodes), and then 100 s at 125°C of OSL (470 nm diodes). Equivalent dose was determined by the single-aliquot regenerative dose (SAR) method (Murray and Wintle, 2000) using a preheat of 240°C for 10s, a test dose of 3.1 Gy, and a cut heat of 200°C. Anomalous fading involving feldspars was removed using the IRSL stimulation to remove most of the feldspar signal, so that the subsequent OSL (post IR blue) signal is free from this influence. A dose recovery test was performed by first zeroing the sample by exposure to light and then administering a known dose. The SAR protocol was then applied to test if the known dose was obtained.

Total OSL dose rates were determined for each sample as the sum of internal radiation from the sherd material, external radiation from surrounding sediments, and incident cosmic radiation. The total dose rate is dominated by internal alpha and beta radiation, contributing ~75% of the dose. Internal alpha, beta, and gamma dose rates on the sherds were determined using alpha counting and flame photometry following Feathers (2009). Radioactive component concentrations (U, Th, K) were translated into dose rates following Adamiec and Aitken (1998). Sediments from the Zhongba site were not measured with the ceramic sherds, so the external radiation dose rate was estimated using the radioactive component concentrations of eolian sediments from an archaeological site on the northeastern Tibetan Plateau (Sun et al., 2010) using a conservative 25% error. While there is no reason to believe the sediments in this site are representative of all Tibet, the resulting error in the total dose rate is small because of the dominance of the internal radiative dose within the sherds. The external dose rate from sediments is dominated by gamma radiation due to the short mean free path of alpha and beta particles relative to the sampling distance of >2 mm from the sherd exterior. At the high altitude of our study area and in a surface context, the modeled cosmic ray dose rate makes up almost half the external dose rate, further meaning the uncertainty imparted by the sediment gamma dose should be small. Moisture content was estimated as 50 ± 30% of the saturated value for the ceramic sherds, reflecting the

https://doi.org/10.1016/j.yqres.2016.04.001 Published online by Cambridge University Press

Table 1
AMS radiocarbon dates and $\delta^{13}C$ values from Upper Yarlung Tsangpo wetlands deposits

Sample site	Sample ID	Lab number	Sample material	Source	$\delta^{13}C$ (PDB)[a]	^{14}C age ± 1σ (^{14}C yr BP)	2σ calendar age range (cal yr BP)	Median age (cal yr BP)[b]
Zhongba	10-1-1	AA96594	Fibrous organic material	Hudson et al., 2014	−25.0	8790 ± 50	9602–10,146	9870 ± 270
	10-1-1H[c]	AA104256	Fibrous organics humates	This study	−24.6	8390 ± 40	–	–
	10-1-2	AA95308	Bulk organic sediment	Hudson et al., 2014	−23.9	5800 ± 40	6493–6716	6600 ± 110
	10-1-2H[c]	AA104257	Bulk sediment humates	This study	−24.0	5170 ± 40	–	–
	10-1-5	AA95306	Articulated bivalve shell	Hudson et al., 2014	−5.7	2550 ± 40	2491–2755	2620 ± 130
	10-4-1	AA94393	Modern aquatic algae	Hudson et al., 2014	−19.8	1310 ± 40	–	–
	10-6a	AA99888	Modern aquatic plants	Hudson et al., 2014	−13.7	Post-bomb	Modern	Modern
	10-8-1	AA104261	Fibrous organic material	This study	−25.8	6500 ± 30	7325–7474	7400 ± 80
	10-8-2H	AA104262	Bulk sediment humates	This study	−24.3	3150 ± 30	3260–3449	3350 ± 100
	10-8-4H	AA104263	Bulk sediment humates	This study	−23.8	2070 ± 40	1935–2144	2040 ± 100
	10-9-1	AA95305	Bulk organic sediment	Hudson et al., 2014	−24.5	2050 ± 30	1931–2115	2020 ± 90
	10-9-1H	AA104258	Bulk sediment humates	This study	−24.4	2030 ± 30	1898–2105	2000 ± 100
	10-9b-3	AA95304	Bulk organic sediment	Hudson et al., 2014	−24.4	3180 ± 30	3356–3456	3410 ± 50
	10-9b-4	AA96593	Carbonate sediment (marl)	Hudson et al., 2014	−7.2	1390 ± 30	1277–1348	1310 ± 40
	10-11-1H	AA104264	Bulk sediment humates	This study	−23.9	2660 ± 20	2746–2836	2790 ± 40
	10-13-1	AA106481	Bulk organic sediment	This study	−26.3	7070 ± 40	7800–7972	7890 ± 90
	10-13-1H[c]	AA104265	Bulk sediment humates	This study	−24.7	6610 ± 40	–	–
	10-13-2H	AA104267	Bulk sediment humates	This study	−24.6	1190 ± 30	1005–1229	1120 ± 110
	13-2-1	AA104245	Fibrous organic material	This study	−24.6	5880 ± 40	6626–6794	6690 ± 100
	13-2-1H[c]	AA104259	Fibrous organics humates	This study	−26.0	5500 ± 40	–	–
	13-2-2	AA104246	Fibrous organic material	This study	−25.5	2740 ± 30	2765–2920	2840 ± 80
	13-2-2H	AA104260	Fibrous organics humates	This study	−25.1	2760 ± 30	2779–2941	2860 ± 80
Tsangpo 18	18-1a	AA82161	Puppilidae shell	This study	−7.1	3700 ± 30	3930–4148	4040 ± 110
	18-1dH	AA82157	Bulk organic humates	This study	−23.6	4700 ± 30	5321–5579	5450 ± 130
	18-1e	AA107433	Bulk organic sediment	This study	−25.0	4080 ± 30	4445–4806	4630 ± 180
	18-1eH[c]	AA82158	Bulk organic humates	This study	−23.6	3960 ± 40	–	–
	18-2a	AA82152	*Radix* sp. shell	Hudson et al., 2014	−11.1	7070 ± 50	7792–7983	7890 ± 100
	18–2[c]	AA107434	Bulk organic sediment	This study	−24.5	4930 ± 30	5600–5720	5660 ± 60
	18-2cH[c]	AA82160	Bulk organic humates	Hudson et al., 2014	−23.7	4710 ± 40	–	–
	18-2d	AA82153	Puppilidae shell	Hudson et al., 2014	−6.8	2570 ± 30	2508–2758	2630 ± 120
	18-2e	AA82154	Succineidae shell	Hudson et al., 2014	−5.6	2700 ± 30	2755–2854	2800 ± 50
Tsangpo 20	20a	AA107431	Bulk organic sediment	This study	−25.8	8670 ± 30	9546–9687	9620 ± 70
	20aH[c]	AA82156	Bulk organic humates	This study	−25.0	8630 ± 50	–	–
	20b	AA107432	Bulk organic sediment	This study	−25.6	9200 ± 50	10,245-10,500	10,370±130
	20bH[c]	AA82159	Bulk organic humates	This study	−25.0	8690 ± 50	–	–
Kay Lak	10-3-1[c]	AA106478	Bulk organic sediment	This study	−23.3	5430 ± 30	–	–
	10-3-1H	AA104268	Bulk sediment humates	This study	−24.0	5750 ± 30	6468–6639	6550 ± 90
	13-1-1	AA105972	Succineidae shell	This study	−4.2	3710 ± 60	3893–4236	4060 ± 170
	13-1-3	AA105973	Puppilidae shell	This study	−6.8	2310 ± 50	2154–2465	2310 ± 160
	13-3-1	AA106482	Bulk organic sediment	This study	−23.8	5440 ± 60	6016–6395	6210 ± 190
Yulai Cun	13-1-1[c]	AA106480	Bulk organic sediment	This study	−24.0	3950 ± 30	–	–
	13-1-1H	AA105804	Bulk sediment humates	This study	−24.0	4530 ± 40	5046–5314	5180 ± 130
	13-1-4	AA105805	Pond bank plant stems	This study	−24.2	Post-bomb	–	Modern
	13-1-5[c]	AA106479	Bulk organic sediment	This study	−24.1	3110 ± 30	–	–
	13-1-5H	AA104266	Bulk sediment humates	This study	−24.1	4250 ± 30	4666–4865	4770 ± 100
	13-2-4H	AA105806	Bulk sediment humates	This study	−24.2	4350 ± 40	4843–5039	4940 ± 100

[a] Values in per mil (‰) versus Pee Dee Belemnite (PDB); 2σ measurement error is ±0.2‰.
[b] Median age is the simple median of the 2σ calendar range with error being one-half the calendar range, both rounded to the nearest 10 cal yr.
[c] Sample ^{14}C dates from the paired dating experiment determined to be unreliable were not calibrated or included in the stratigraphic results.

variability of the surface context. Saturated moisture contents were measured for each sherd by comparing the dry and saturated sample mass. Ages for the sherd are calculated by dividing the equivalent dose by the total dose rate. All error terms are reported at 2σ, and the 'present' reference for the ages has been corrected to AD 1950 for comparison to ^{14}C ages.

Dating results

We present a total of forty-six ^{14}C ages on natural materials and two luminescence ages on ceramic sherds. The following section presents the ages, discusses the results of the humate-residue ^{14}C dating experiment, and discusses the potential for 'hard water' reservoir effects on the ^{14}C ages. We then place the most reliable ages into the stratigraphic results and discuss them in the following section.

Humate versus residue fraction results

The diffuse organics and root contamination in the paleowetlands deposits makes isolation and concentration of primary organic matter for dating difficult. We extracted organic matter chemically in the form of NaOH-soluble humates (humic acids), to explore whether dating this fraction provided a viable method to minimize the effect of young root contamination and concentrate the primary organic matter. Typical procedure for dating of organics treats humates as a contaminant, and therefore only the insoluble residue fraction is retained for dating. This is because humates are relatively soluble, and therefore mobile within sediment sections after deposition, which often leads to addition of secondary humates from other carbon sources to the primary material. Self-humification, or the *in situ* decomposition of primary organic matter, however, can create primary humates of the same

https://doi.org/10.1016/j.yqres.2016.04.001 Published online by Cambridge University Press

^{14}C content, thus providing reliable ^{14}C ages. The vegetal material composing modern roots is relatively insoluble, so when complete mechanical separation of roots is not possible, extraction of humates may provide reliable ages where primary humates are the dominant fraction.

We analyzed thirteen pairs of humate/residue ages in this study that provide mixed results for the efficacy of the humate dating procedure in the YT wetlands sediments. The ages for these sample pairs range from 2030 ± 30 to 8690 ± 50 ^{14}C yr BP for humates and 2050 ± 30 to 9200 ± 50 ^{14}C yr BP for residues, respectively (Table 2). Four pairs (Zhongba 10-1-1, 10-1-2, 10-9-1, Tsangpo 18-2c) consist of previously published residue ages (Hudson et al., 2014) compared to new humate fraction ages for the same samples. Three new pairs come from the Zhongba site, one from Tsangpo 18, two from Tsangpo 20, one from Kay Lak 10-3, and two from Yulai Cun 13-1. For the two youngest pairs (Zhongba 10-9-1, 10-9-1H; 13-2-2, 13-2-2H) and the uppermost pair from Tsangpo 20 (20a, 20aH), the humate and residue ages overlap within 1σ error, indicating the humate fraction is composed almost entirely of the same self-humified primary organic matter as the residue. In all three cases, the black mat horizons do not contain significant modern roots and are not below younger wetlands deposits in the sediment sections (Figs. 4 and 5). These two factors, in conjunction with <3000 yr exposure to weathering processes for the younger samples, may have limited contamination by young humates or roots. Although Tsangpo 20a is one of the oldest samples, it is overlain by sterile alluvial gravel, which may have limited its contamination despite the long weathering period. For the remaining ten pairs, the humate fractions range between 120 ± 70–630 ± 80 ^{14}C yr younger and 320 ± 60–1140 ± 60 ^{14}C yr older than the residue fractions (Table 2). The seven sample pairs where humate ages are younger than the residues came from the Zhongba, Tsangpo 18 and Tsangpo 20 sites (Table 2), where they were sampled from horizons overlain by significant thickness of younger paleowetlands sediments. At these sites we report the older residue ages in the stratigraphic descriptions below, assuming the humate samples incorporate some fraction of mobile young carbon brought in solution by infiltration of water through the higher part of the sediment sections.

The three pairs where humate ages are older than residue ages were sampled from Kay Lak 10-3 and Yulai Cun 13-1 (Figs. 5 and 6D), where the wetlands horizons are near or at the modern surface and subject to extensive modern root contamination. It is likely that even with the root removal procedure, root detritus was impossible to eliminate completely by mechanical means. Some root material was likely incorporated into the residue fractions dated, resulting in erroneously young ages. For these pairs, we report the older humate ages because isolating the humate fraction likely limited contamination from insoluble modern root material, and the sampled horizons are not overlain by younger black mats. Based on the anomalously young humate results for the majority (n = 7) of sample pairs, we still view these humate ages as minimum ages. To summarize, dating of humates can clearly provide reliable ^{14}C ages for black mats and eliminate fine root contamination for samples <3000 yr in age. Humate ages are also viable for older deposits with limited organic-rich sedimentary overburden, but must be interpreted with caution. Downward transport of younger soluble humates into older black mats from overlying organic-rich deposits may result in ^{14}C contamination and erroneous younging of ages.

Reservoir effect considerations

Previous study of the Zhongba site (Hudson et al., 2014) indicated that ^{14}C reservoir effects significantly affected modern

Table 2
Paired black mat insoluble residue/humate ^{14}C dating results.

Sample site	Sample ID	Lab number	Sample material	δ^{13}C (PDB)	^{14}C age ± 1σ (^{14}C yr BP)	Age difference (residue-humate)
Zhongba	10-1-1	AA96594	Fibrous organic material	−25.0	8790 ± 50	
	10-1-1H	AA104256	Fibrous organics humates	−24.6	8390 ± 40	400 ± 90
	10-1-2	AA95308	Bulk organic sediment	−23.9	5800 ± 40	
	10-1-2H	AA104257	Bulk sediment humates	−24.0	5170 ± 40	630 ± 80
	10-9-1	AA95305	Bulk organic sediment	−24.5	2050 ± 30	
	10-9-1H	AA104258	Bulk sediment humates	−24.4	2030 ± 30	20 ± 60
	10-13-1	AA106481	Bulk organic sediment	−24.1	7070 ± 40	
	10-13-1H	AA104265	Bulk sediment humates	−24.7	6610 ± 40	460 ± 80
	13-2-1	AA104245	Fibrous organic material	−24.6	5880 ± 40	
	13-2-1H	AA104259	Fibrous organics humates	−26.0	5500 ± 40	380 ± 80
	13-2-2	AA104246	Fibrous organic material	−25.5	2740 ± 30	
	13-2-2H	AA104260	Fibrous organics humates	−25.1	2760 ± 30	−20 ± 60
Tsangpo 18	18-1e	AA107433	Bulk organic sediment	−25.0	4080 ± 30	
	18-1eH	AA82158	Bulk organic humates	−23.6	3960 ± 40	120 ± 70
	18-2c	AA107434	Bulk organic sediment	−24.5	4930 ± 30	
	18-2cH	AA82160	Bulk organic humates	−23.7	4710 ± 40	220 ± 70
Tsangpo 20	20a	AA107431	Bulk organic sediment	−25.8	8670 ± 30	
	20aH	AA82156	Bulk organic humates	−25.0	8630 ± 50	40 ± 80
	20b	AA107432	Bulk organic sediment	−25.6	9200 ± 50	
	20bH	AA82159	Bulk organic humates	−25.0	8690 ± 50	510 ± 100
Kay Lak	10-3-1	AA106478	Bulk organic sediment	−23.3	5430 ± 30	
	10-3-1H	AA104268	Bulk sediment humates	−24.0	5750 ± 30	−320 ± 60
Yulai Cun	13-1-1	AA106480	Bulk organic sediment	−24.0	4150 ± 30	
	13-1-1H	AA105804	Bulk sediment humates	−24.0	4530 ± 40	−380 ± 70
	13-1-5	AA106479	Bulk organic sediment	−24.1	3110 ± 30	
	13-1-5H	AA104266	Bulk sediment humates	−24.1	4250 ± 30	−1140 ± 60

https://doi.org/10.1016/j.yqres.2016.04.001 Published online by Cambridge University Press

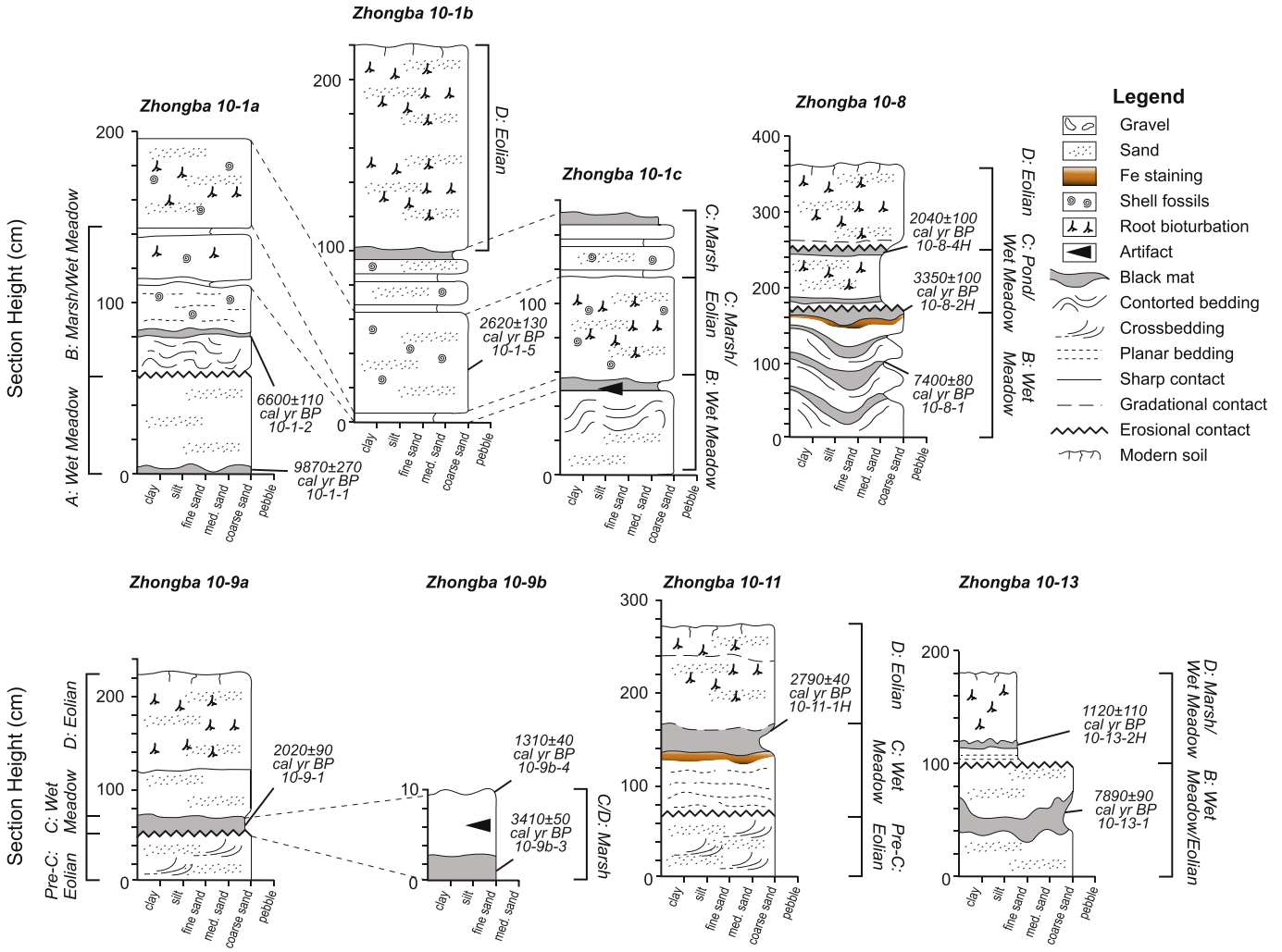

Figure 4. Zhongba locality paleowetlands stratigraphic sections. Sections are grouped by study site. Facies interpretations and unit boundaries for Units A-D are indicated to the side of each section. Units without constraining ages are designated pre- or post- with respect to the over or underlying unit (e.g. Pre-C), respectively. Zhongba 10-1 and 10-9 sections modified from Hudson et al. (2014).

aquatic samples, causing the ^{14}C ages to appear older than the true age of deposition by between 0 and 1370 ^{14}C yr (Table 1). This effect was prevalent in both modern and fossil aquatic carbonate materials (shells, marls), and so these materials were avoided where possible in the current study. Mollusk shells dated here are instead of the semi-aquatic Succineidae and terrestrial Pupillidae genera, which spend part or all of the time living terrestrially. These taxa build their shells from consumed organic carbon rather than dissolved inorganic carbon (DIC) in water (Pigati et al., 2004, 2011), and are therefore less likely to produce ^{14}C-deficient carbonate. Some of the previously published mollusk shell ages were deemed reliable, based on good agreement with black mat ages, and we retain these ages in the stratigraphic sections below, viewing them as maximum-limiting ages. The rest of the ^{14}C chronology is composed of black mat residue and humate ages to further minimize reservoir effect uncertainties. Although aquatic organic matter exhibited a reservoir effect in one Zhongba site (Hudson et al., 2014), a key observation from the previous study was again the similarity in ages derived from black mats from multiple sections, indicating common periods of wet conditions between sites. The data presented here provide an additional test of this observation, and show excellent agreement in age between sections and localities within all stratigraphic units. The magnitude of reservoir effects varies from 0 to 1370 ^{14}C yr between three different ponds within the Zhongba site alone (Hudson et al., 2014). It is highly unlikely to observe good agreement between ages of wetlands units across localities spanning hundreds of kilometers if this level of variability commonly affects the wetlands deposits.

$\delta^{13}C$ values provide additional evidence for reliability of black mat ages (Table 1). Humate and residue $\delta^{13}C$ values range between −23.3‰ and −26.3‰ (versus Pee Dee Belemnite, PDB), consistent with a C_3 terrestrial vegetation source (Deines, 1980). These plants draw CO_2 for photosynthesis from the atmosphere rather than a potentially ^{14}C-deficient aquatic source. One modern sample (YLC13-1-4) of emergent plant stems from the margin of a wetlands pond at Yulai Cun yielded a $\delta^{13}C$ value of −24.2‰ and a modern ^{14}C age, supporting this conclusion. Formation of black mats from dominantly terrestrial vegetation is consistent with findings for similar deposits in western North America (Harris-Parks, 2016). In contrast, the modern aquatic plant samples dated by Hudson et al. (2014) are clearly distinguished from black mats and modern pond margin plants by much higher $\delta^{13}C$ values of −13.7‰ (13-6a) and −19.8‰ (10-4-1), indicating formation from aquatic carbon sources (Table 1). This evidence for terrestrial sample origin, in conjunction with demonstrated age agreement

https://doi.org/10.1016/j.yqres.2016.04.001 Published online by Cambridge University Press

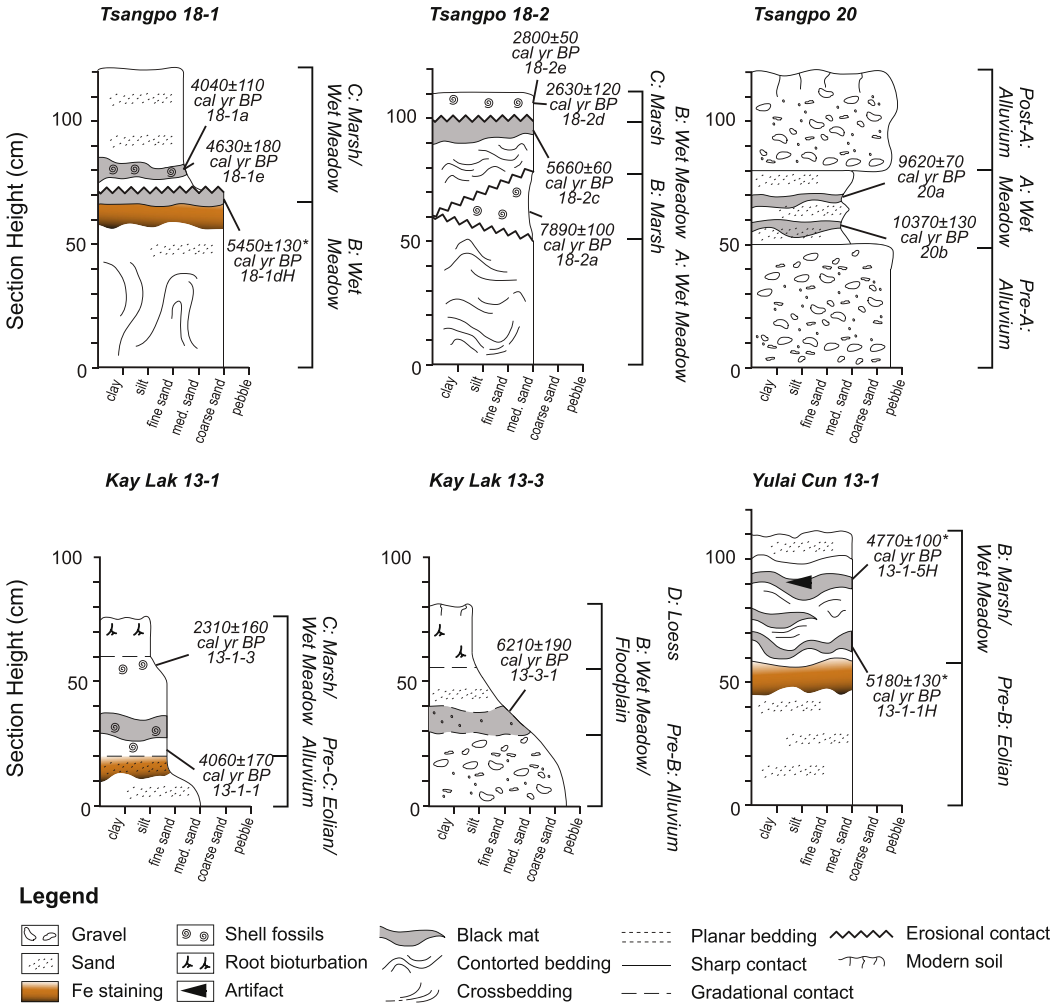

Figure 5. Tsangpo, Kay Lak and Yulai Cun locality stratigraphic sections. Sections are grouped by study site. Facies interpretations and unit boundaries for Units A-D are indicated by brackets to the side of each section. Units without constraining ages are designated pre- or post- with respect to the over or underlying unit (e.g. Pre-C), respectively. Ages denoted with an asterisk (*) are minimum ages, based on dating of humates. Tsangpo 18-2 section modified from Hudson et al. (2014).

between sites, provides confidence that reservoir effects do not significantly affect the black mat ^{14}C ages presented in this study.

Luminescence dating results

Two sherds (UW2676, UW2679; Table 3) were collected in surface context from Zhongba 10-9 within the Zhongba locality, for which residue ^{14}C ages have been previously reported (Hudson et al., 2014; Table 1). Both have similar characteristics: unmarked, unpainted with brick red color, coarse sand temper and red matrix. These two sherds yield OSL ages of 1330 ± 180 yr (UW2676) and 1060 ± 160 yr (UW2679), respectively (Table 3).

Stratigraphic section results

We present fourteen stratigraphic sections with ^{14}C age control distributed between the Zhongba (Fig. 4), Kay Lak, Yulai Cun, Tsangpo 18, and Tsangpo 20 study localities (Fig. 5). For Zhongba, three new sections supplement the five previously published in Hudson et al. (2014). These previous five are reproduced here for comparison, but not described in detail. All Zhongba sections and other sample sites are located in interdune depressions along a southwest-northeast trending transect near the north side of the dunefield that makes up the Zhongba locality (Fig. 3). Two new sections come from the Kay Lak valley, two from Tsangpo 18, one from Tsangpo 20, and one from Yulai Cun. Tsangpo 18-2, also reproduced from Hudson et al. (2014), is included in Fig. 5, but not discussed in detail. Based on the most reliable ^{14}C ages determined in the prior section, the sections contain twenty-six ^{14}C ages, and four additional ages come from wetlands horizons found at the modern ground surface. ^{14}C ages from Hudson et al. (2014) have been recalibrated using the IntCal13 calibration curve (Reimer et al., 2013) for consistent comparison to the new ages. The total age range for these twenty-eight samples is 1120 ± 110–10,370 ± 130 cal yr BP (Table 1).

Zhongba sections and surface exposures

Zhongba 10-8 consists of three units that are a total of 360 cm thick. The lowermost unit is calcareous, silty sand with contorted bedding and contains three black mats. It is capped by an erosional unconformity with Fe-oxidation staining below the contact. The middle black mat horizon in this unit yields a plant macrofossil residue age of 7400 ± 80 cal yr BP (10-8-1), and the uppermost mat yields a humate age of 3350 ± 100 cal yr BP (10-8-2H). The middle unit consists of silty, calcareous coarse sand with wavy planar bedding. There are two black mats within the unit, which is capped by an erosional unconformity. The upper mat yields a humate age of

https://doi.org/10.1016/j.yqres.2016.04.001 Published online by Cambridge University Press

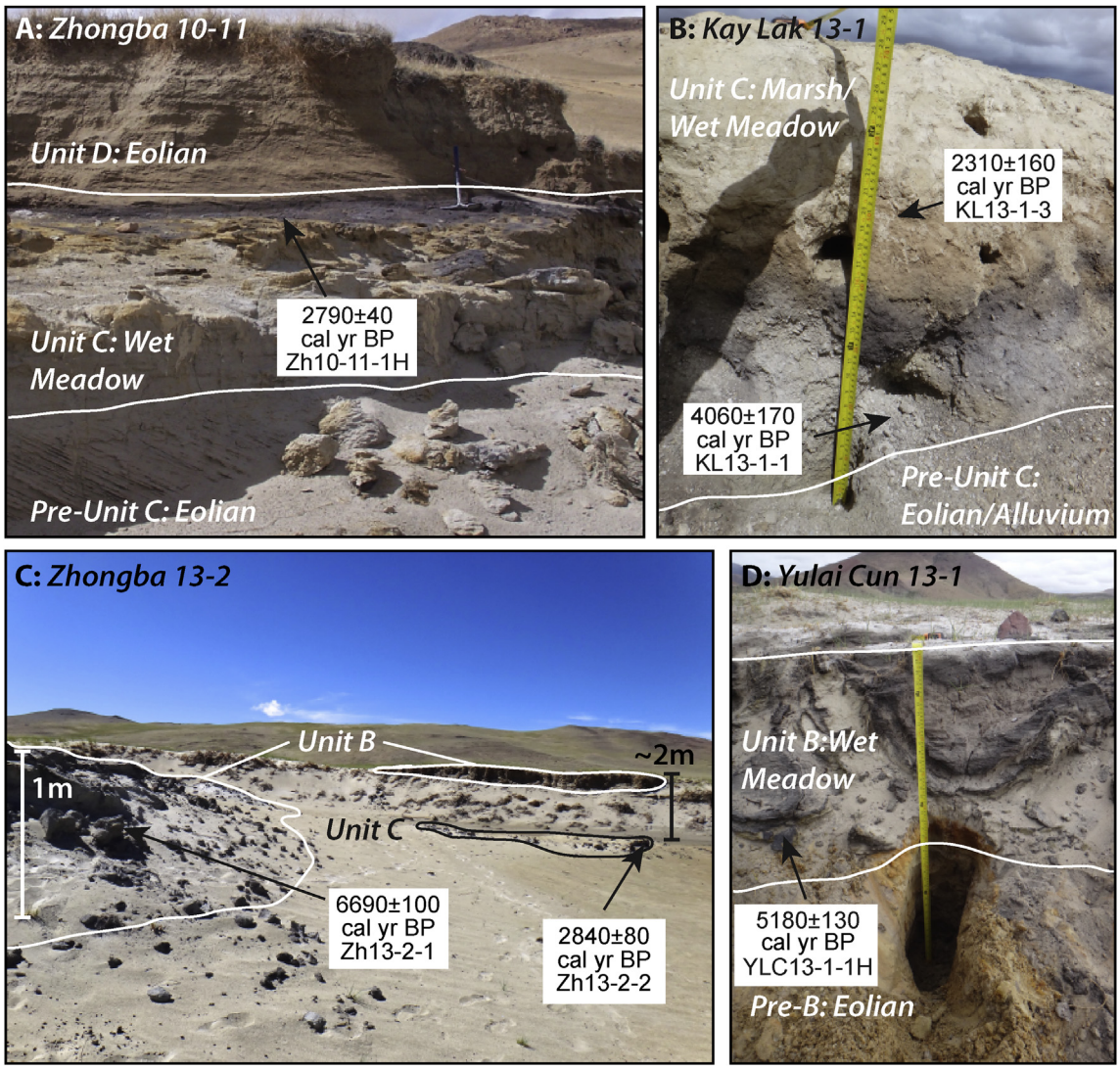

Figure 6. Photographs of selected stratigraphic sections. Unit (A–D) and/or facies interpretation are labeled for each. Unit boundaries are delineated by thick lines. Locations and ages of ^{14}C samples are indicated with arrows. A – Zhongba 10-11, section is 180 cm in height. B – Kay Lak 13-1, section is 75 cm in height. C – Zhongba 13-2, note inset position of younger Unit C into the depression below eroding Unit B. Height of Unit B outcrop in foreground is approximately 1 m. Height difference between Unit B outcrop and depression bottom in background is approximately 2 m. D – Yulai Cun 13-1, section is 110 cm in height.

2040 ± 100 cal yr BP (10-8-4H). The uppermost unit consists of massive, noncalcareous coarse sand. It contains no fossil organic matter, and is extensively bioturbated by modern roots.

Zhongba 10-11 consists of three units that are a total of 270 cm thick (Figs. 4 and 6A). The lowermost unit is slightly calcareous coarse sand with trough crossbedding, capped by an erosional unconformity. The middle unit is calcareous with wavy planar bedding, capped by a thick black mat with Fe-oxidation staining at the base. This mat yields a humate age of 2790 ± 40 cal yr BP (10-11-1H). The uppermost unit begins above a gradational contact, and consists of noncalcareous, root bioturbated massive sand.

Zhongba 10-13 consists of two units that are a total of 180 cm thick. The lower unit is calcareous coarse sand with contorted bedding. This unit has a black mat in the center yielding a residue age of 7890 ± 90 cal yr BP (10-13-1). The upper unit begins above an erosional unconformity, and is weakly bedded sandy silt. It is highly calcareous with root bioturbation. A thin organic horizon 20 cm above the lower contact yields a humate age of 1120 ± 110 cal yr BP (10-13-2H).

Zhongba 13-2 consists of two surface exposures of black mat horizons within an interdune depression. Zhongba 13-2-1 was sampled from a prominent black mat exposed in the eroding wall of the depression approximately 2 m above the modern water level

Table 3
Luminescence dating results for Zhongba ceramic sherds.

Sample ID	^{238}U (ppm)	^{233}Th (ppm)	K (%)	Alpha dose rate (Gy/ka)	Beta dose rate (Gy/ka)	Gamma dose rate (Gy/ka)	Cosmic dose rate (Gy/ka)	Total dose rate (Gy/ka)	Equivalent dose (Gy)	OSL age (cal yr BP)[a]
UW2676	3.48 ± 0.25	10.68 ± 1.39	2.71 ± 0.10	0.67 ± 0.05	2.77 ± 0.14	0.64 ± 0.11	0.55 ± 0.11	4.64 ± 0.20	6.44 ± 0.14	1390 ± 80
UW2679	2.68 ± 0.25	15.93 ± 1.73	2.52 ± 0.12	0.56 ± 0.07	2.62 ± 0.16	0.63 ± 0.08	0.55 ± 0.11	4.36 ± 0.23	4.89 ± 0.19	1060 ± 80

[a] Where cal yr BP denotes age before AD 1950, for comparison to ^{14}C ages. All errors are reported at 2σ.

https://doi.org/10.1016/j.yqres.2016.04.001 Published online by Cambridge University Press

(Fig. 6C). This yields a residue age of 6690 ± 100 cal yr BP. Zhongba 13-2-2 was sampled from a black mat exposed in the bottom of the depression, erosionally inset within Zhongba 13-2-1. This yields a residue age of 2840 ± 80 cal yr BP.

Tsangpo sections

Tsangpo 18-1 consists of two units that are a total of 120 cm thick (Fig. 5). The lowermost unit consists of noncalcareous organic-rich coarse sand with contorted bedding. The upper 15 cm of this unit contains a black mat with extensive Fe-staining and yields a humate minimum age of 5450 ± 130 cal yr BP (18-1dH). The overlying unit is above an erosional contact and also consists of organic-rich, bedded coarse sand. A thin black mat horizon 25 cm above the lower contact yields a residue age of 4630 ± 180 cal yr BP (18-1e). Puppilidae mollusk shells within the organic horizon yields a similar age of 4040 ± 110 cal yr BP (18-1a).

Tsangpo 20 consists of three units that are a total of 120 cm thick. The lower unit is coarse, angular cobble gravel with a sandy matrix. The middle unit consists of planar-bedded, silty sand with two black mat horizons yielding residue ages of 9620 ± 70 cal yr BP (20a) and 10,370 ± 130 cal yr BP (20b). The upper unit is composed of dispersed cobbles in a silt matrix with coarse prismatic peds indicating post-depositional soil development.

Kay Lak sections and surface exposure

Kay Lak 13-1 consists of two units that are a total of 75 cm thick. The lower unit consists of noncalcareous medium sand grading up to fine sand. The upper contact is gradational and extensively Fe-stained. The upper unit consists of highly calcareous sandy silt grading upward to silty marl with modern root bioturbation, indicating wetlands desiccation. It contains an organic horizon 20 cm above the lower contact and fossil aquatic (*Gyraulus* sp.), semi-aquatic (Succineidae) and terrestrial (Pupillidae) mollusks dispersed throughout. A Succineidae shell 10 cm above the lower contact yields an age of 4060 ± 170 cal yr BP (13-1-1). A Pupillidae shell from 25 cm below the upper surface yields an age of 2310 ± 160 cal yr BP (13-1-3).

Kay Lak 13-3 consists of three units that are a total of 80 cm thick. The lower unit consists of matrix-supported sandy gravel grading upward to gravelly medium sand with a gradational upper contact. The middle unit contains a diffuse organic horizon at the base grading upward from medium sand to silty sand. The organic horizon yields a residue age of 6210 ± 190 cal yr BP (13-3-1). The upper unit is silty marl with modern root bioturbation.

Kay Lak 10-3 is a surface exposure of a black mat horizon at ground level in the central Kay Lak valley, consisting of organic-rich medium sand and containing a single *in situ* obsidian flake. The black mat yields a humate minimum age of 6550 ± 90 cal yr BP (10-3-1H).

Yulai Cun sections and surface exposure

Yulai Cun 13-1 consists of three units of medium sand that are a total of 122 cm thick (Figs. 5 and 6B). The lower unit is massive, noncalcareous and unconsolidated, with diffuse organic matter and extensive Fe-oxidation staining at the upper contact. The middle unit is mildly calcareous with contorted bedding and several diffuse black mats. Two plain red ceramic sherds with coarse sand temper were recovered *in situ* from the middle of this unit. The lowermost mat yields a humate minimum age of 5180 ± 130 cal yr BP (13-1-1H), while the uppermost horizon, which was sampled adjacent to the sherds, yields a humate minimum age of 4770 ± 100 cal yr BP (13-1-5H), providing upper and lower limiting age constraints for the artifacts. The upper unit is highly calcareous with contorted bedding and modern root bioturbation.

Yulai Cun 13-2 is a surface exposure of a black mat horizon consisting of mildly calcareous organic-rich sand. It is located approximately 30 m southeast from Yulai Cun 13-1 on the opposite margin of a modern interdune pond. The black mat yields a humate minimum age of 4940 ± 100 cal yr BP (YLC 13-2-4H).

Regional stratigraphic framework for deposits (Units A–D)

Synthesizing the stratigraphic and dating results, the wetlands sedimentary record can be divided into four units A–D from oldest to youngest, defined by distinct age ranges, stratigraphic relationships, and sedimentary features (Fig. 7, Table 4). The unit interpretations for individual intervals in the sections are labeled next to each section (Figs. 4–6). Each unit is defined first as a recurring sedimentary package with clearly observed stratigraphic position relative to the others in the sections in the field. The bounding ages for each unit are then defined by the oldest and youngest ages obtained from sediments within them. Because of the extreme lateral variability of wetlands depositional environments, there are instances where units are missing (e.g. Unit C missing from Zhongba 10-13), stratigraphic breaks may be obscured by sediment deformation, deposition may continue across unit boundaries in time indicating deposition did not cease completely at all locations (e.g. the uppermost black mat in Unit B is younger than the boundary quoted in the text in Zhongba 10-8), and some contacts are likely diachronous. This uncertainty in the unit boundary ages does not affect the overall interpretation of the units appreciably.

Within each unit, the constraining ^{14}C ages have similar, overlapping ages distributed between individual stratigraphic sections, and between the five localities in the study area, which are expressed by the individual and cumulative probability density functions (pdf) for each locality (Fig. 7). Plotting cumulative pdf's provides a graphical display of the overlapping ages, with increased peak height indicating both the number of overlapping ages and the precision of the ^{14}C measurements within a given interval. Therefore, young peaks corresponding to higher precision ages (<3.4 ka) are taller than those during the mid-Holocene which have lower AMS measurement precision (8.0–4.0 ka BP). Peak height is also affected by the shape and precision of the calibration curve (Bleicher, 2013) with no relation to the data, a problem that is especially acute where many ages span a large interval of overlap. The ages considered here are relatively few and have narrow calibrated ranges so that their time spans are limited to discrete periods, and therefore calibration curve shape is a minor contributor to the shape of the cumulative plot. To help identify individual ages, however, we have included 2σ calibration intervals of the radiocarbon ages plotted above the cumulative curve.

Unit A: ca. 10.4–>8.0 ka BP

Unit A is the oldest stratigraphic unit, is early Holocene in age, and is poorly exposed in the study area. It appears at Zhongba in the base of section 10-1a, where it is constrained by a ^{14}C age of 9870 ± 270 cal yr BP, at the base of the section at Tsangpo 18-2 undated, and in the wetlands unit of Tsangpo 20 with ages of 10,370 ± 130 and 9620 ± 70 cal yr BP (Figs. 4 and 5; Hudson et al., 2014). In all locations it is composed of non- or mildly calcareous sand with planar or contorted bedding, and thin black mat horizons. A *Radix* shell maximum age (7890 ± 100 cal yr BP, 18-2a) from a calcareous marsh deposit in Unit B, unconformably overlying Unit A in Tsangpo 18-2, provides a minimum constraint on Unit A, but the exact upper age boundary is unknown. Because *Radix* shells have been shown to be affected by reservoir effects (Hudson et al., 2014), this limiting age could potentially be younger. Two

https://doi.org/10.1016/j.yqres.2016.04.001 Published online by Cambridge University Press

overlapping ^{14}C ages from Unit A at Zhongba and Tsangpo 20 indicate a coherent period of wetlands formation at 9.6 ka BP (Fig. 7). The sedimentary facies resemble Unit B, which unconformably overlies Unit A, suggesting similar environmental conditions, although the unconformity indicates a period of dry climate and erosion separating the two units. Based on the bedding, soft-sediment deformation, and the lack of calcareous sediment, Unit A is dominated by organic-rich wet meadow horizons, interpreted to be deposited in wet conditions. The poor exposure in the study area makes it difficult to fully characterize the range of sedimentary facies and therefore depositional environments. We suggest that lack of exposure is most likely a result of burial beneath the extensive younger deposits rather than an absence of wetlands environments. No artifacts have been found *in situ* within or associated with this unit.

Unit B: ca. 7.9–4.8 ka BP

Unit B is the most commonly exposed unit in the study area, appearing in six sections and three surface exposures at all localities except Tsangpo 20. It is also the most voluminous, forming huge, laterally extensive banks of sediment in the walls of the interdune wetland sites (Figs. 2C and 6C). It ranges roughly in age from 7.9 to 4.8 ka BP. It unconformably overlies Unit A where the contact is exposed (Tsangpo 18-2, Zhongba 10-1), but otherwise forms the oldest identified stratigraphic unit in most sections. The oldest constraining age comes from the base of Zhongba 10-13

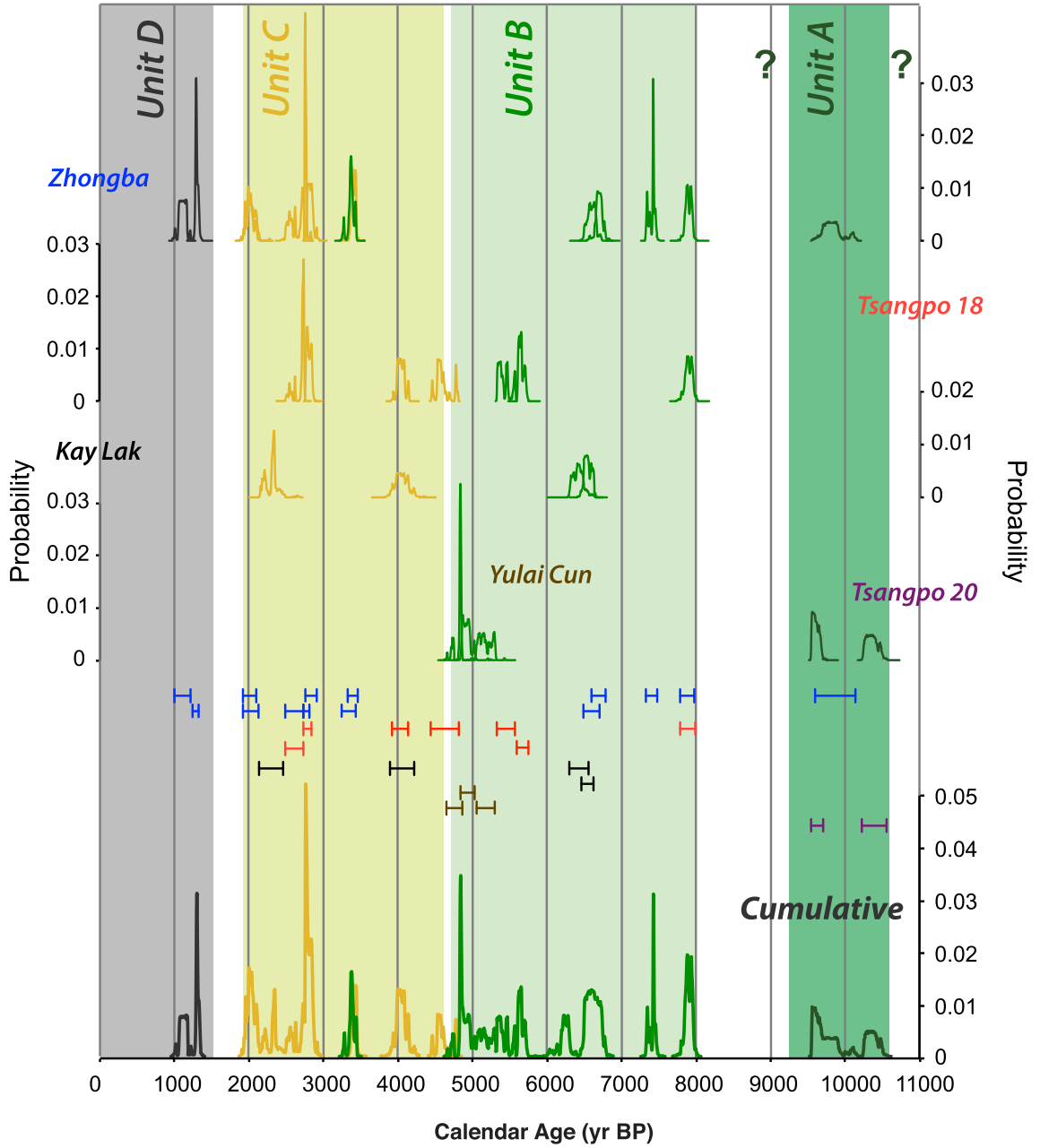

Figure 7. Calibrated ^{14}C age probability density functions for paleowetlands localities. Individual ages for each locality are coded by unit color: dark green – Unit A, light green – Unit B, gold – Unit C, dark gray – Unit D. The cumulative probability distribution is the sum of all ages from all localities, color coded by unit. 2σ calendar age ranges for each age are plotted above the cumulative distribution, color coded by site: blue – Zhongba, red – Tsangpo 18, black – Kay Lak, brown – Yulai Cun, violet – Tsangpo 20. Depositional intervals for major wetlands sedimentary Units A-D are indicated by vertical bars. Unknown upper and lower age boundaries for Unit A are indicated by question marks. (For interpretation of the references to colour in this figure legend, the reader is referred to the web version of this article.)

https://doi.org/10.1016/j.yqres.2016.04.001 Published online by Cambridge University Press

Table 4
Yarlung Tsangpo wetlands stratigraphic unit characteristics.

Unit	Occurrence localities	Stratigraphic position	Age range (ka)	Prominent wet periods (ka)[a]	Sediment characteristics	Depositional environments[b]	Paleoclimate interpretation	Archaeological materials
Unit D	Zhongba	Unconformably or conformably above Units B or C, diachronous lower contact	2.0 ka to present	1.0–1.3 ka	Non calcareous, eolian crossbedding, no black mats or marls	Eolian dunes	Drier than present conditions and of Units A-C	Lithic artifacts and ceramic artifacts in surface context
Unit C	Zhongba, Tsangpo 18, Kay Lak	Unconformably above or erosionally inset into Unit B, Unconformably or conformably below Unit D, diachronous upper contact	4.6–2.0 ka	2.0–2.7 ka, 3.4 ka	Highly calcareous, limited soft sediment deformation, limited black mats, abundant marls and mollusks	Wet meadow < marsh/ pond	Wetter than present conditions, but drier than conditions of Units A, B	Lithic and ceramic artifacts *in situ* (3.4–1.3 ka) and in surface context
Unit B	Zhongba, Tsangpo 18, Kay Lak, Yulai Cun	Above Unit A, unconformably below or in erosional contact with Units C or D	7.9–4.8 ka	4.8–5.2 ka, 6.6 ka, 7.9 ka	Mildly calcareous, extensive soft sediment deformation, extensive black mats, limited marls and mollusks	Wet meadow > marsh/ pond	Wet monsoon conditions overall, but variable wetness over time interval, similar to conditions of Unit A	Lithic and ceramic artifacts *in situ* (6.6–2.6 ka BP) and in surface context
Unit A	Zhongba, Tsangpo 18, Tsangpo 20	Lowermost unit, below Unit B, but poorly exposed in the study area	10.4–>8.0 ka	10.4 ka, 9.6 ka	Non-calcareous, bedded sands, soft sediment deformation	Wet meadow	Wet monsoon conditions, similar to conditions of Unit B	No artifacts recovered *in situ* or clearly associated

[a] Prominent wet periods are defined by overlapping 2σ calendar dates in multiple stratigraphic sections and/or localities, indicating regional wetlands deposition.
[b] Depositional environment interpretations follow the framework and descriptions for desert wetlands of Pigati et al. (2014).

(7890 ± 90 cal yr BP, 10-13-1), and the youngest from Yulai Cun 13-1 (4770 ± 100 cal yr BP, 13-1-5H). A lower bounding age from a *Radix* shell in Tsangpo 18-2 (7890 ± 100 cal yr BP, 18-2a) is identical, but is viewed as maximum limiting age because of the potential for an aquatic reservoir effect. The age of the uppermost black mat in Unit B in Zhongba 10-8 is too young to fall in this interval (3350 ± 100 cal yr BP, 10-8-2H), complicating this interpretation. It is possible that this black mat falls above an unrecognized unconformity in the highly contorted sediments or that wetlands formation did not cease completely at this location between the formation of Units B and C. We choose to place the upper boundary of Unit B at 4.8 ka BP because multiple ages fall in the range 4.6–4.0 ka at Tsangpo 18-1 above a prominent unconformity with dated Unit B sediments. Shells at the base of the wetlands Unit C in Kay Lak 13-1 date to 4.0 ka BP and also overlie sterile eolian sediments indicating dry prior conditions.

The ^{14}C ages within Unit B indicate coincident periods of black mat formation between Zhongba and Tsangpo 18 at 7.9 ka BP, Zhongba and Kay Lak at 6.6 ka BP, and Tsangpo 18 and Yulai Cun at 5.4 to 4.8 ka BP (Fig. 7). The thickness and sedimentary facies of this unit are characterized by high lateral variability both within individual sites and across the study area. Thicknesses range from <20 cm in the Kay Lak valley to 2 m in section Zhongba 10-8. It is mildly calcareous overall, and sedimentary facies include eolian crossbedded sands, organic-rich silty sands, and highly calcareous marls containing abundant mollusks. The bedding within the entirety of the unit is contorted at the decimeter to meter scale, particularly at the interdune sites (Fig. 2C). Overall, Unit B represents a period of elevated water tables above modern in the upper YT valley, characterized by the most expansive perennial networks of marshes, wet meadows, and ponds with increased plant cover. In the Kay Lak valley, the organic-rich deposits form along the edges of currently ephemeral stream channels and in isolated surface patches (Figs. 2D and 6B), suggesting higher streamflow and more vegetation cover on the valley floor. The sedimentologic diversity of the unit overall suggests high hydrologic variability, with many discrete wet and dry periods. This unit contains rare lithic and ceramic artifacts *in situ* at Zhongba 10-1c, Kay Lak 10-3, and Yulai Cun 13-1, and on the surface near the stream channel at Kay Lak 13-3.

Unit C: ca. 4.6–2.0 ka BP

Unit C dates to the late Holocene, and is only found locally in relatively isolated patches. It is particularly well exposed in several sections at the Zhongba locality and at Tsangpo 18, where it unconformably overlies Unit B. In some cases it is erosionally inset into Unit B (e.g. Tsangpo 18-2) or deposited below it in elevation within the interdune depressions (e.g. Zhongba 13-2; Fig. 6C). It ranges in age from 4.6 to 2.0 ka BP, with the oldest constraining age from Tsangpo 18-1 (4630 ± 180 cal yr BP, 18-1e) and the youngest from Zhongba 10-13 (1120 ± 110 cal yr BP, 10-13-2H). However, the upper contact is diachronous and gradational with Unit D above, and Unit C terminates by 2.0 ka BP in all but two sections (Zhongba 10-9, 10-13). We have chosen to place the boundary at ~2.0 ka BP for this reason. Coincident periods of black mat formation occur between Kay Lak 13-1 and Tsangpo 18-1 at 4.6–4.0 ka BP, Zhongba and Tsangpo 18 at 2.7–2.6 ka BP, and in multiple sections at Zhongba at 3.4, 2.0 ka BP (Fig. 7). Like Unit B, Unit C varies widely in thickness and sedimentary makeup, but is in general <50 cm thick. It is highly calcareous throughout, containing abundant mollusk fossils, with more silty marl horizons than Unit B, and thinner black mat horizons with wavy planar or massive bedding. Relative to Unit B, this unit suggests a lower water table, but wetter conditions than modern. During the deposition interval for Unit C, the interdune wetlands were characterized by fewer wet meadows, evidenced by

https://doi.org/10.1016/j.yqres.2016.04.001 Published online by Cambridge University Press

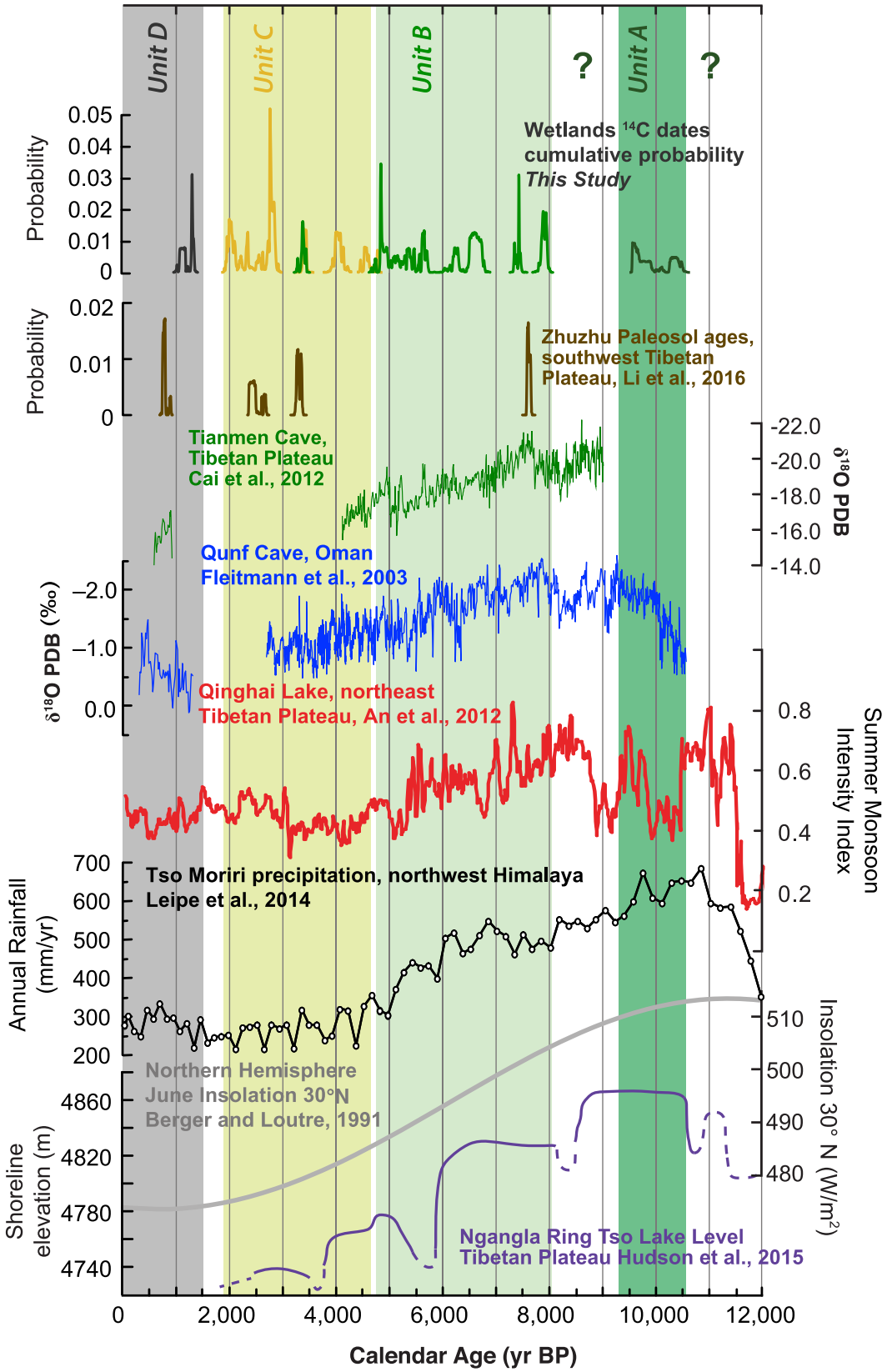

Figure 8. Cumulative probability density function for paleowetlands ages (dark green – Unit A, light green – Unit B, gold – Unit C, dark gray – Unit D) compared to regional paleoclimate records. Locations for records are shown in Fig. 9. Citations for individual records are: Zhuzhu dune paleosol ^{14}C ages (brown, Li et al., 2016), Tianmen Cave speleothem $\delta^{18}O$ record (green, Cai et al., 2012), Qunf Cave speleothem $\delta^{18}O$ record (blue, Fleitmann et al., 2003), Qinghai Lake core-based summer monsoon intensity index (based on percent carbonate and percent total organic carbon), Tso Moriri lake core pollen precipitation reconstruction (black, Leipe et al., 2014), Northern Hemisphere June solar insolation 30°N (light gray, Berger and Loutre, 1991), Ngangla Ring Tso lake level reconstruction (violet, Hudson et al., 2015). Time intervals represented by wetlands Units A-D are shown by vertical bars, question marks denote uncertain age limits for Unit A. (For interpretation of the references to colour in this figure legend, the reader is referred to the web version of this article.)

https://doi.org/10.1016/j.yqres.2016.04.001 Published online by Cambridge University Press

thinner, fewer organic horizons, and were limited to isolated marshes in dune depressions, indicated by the abundant marls and mollusks. Unit C also contains a lithic artifact *in situ* at Zhongba 10-9b, and lithics and ceramics in surface context at Zhongba 10-9b as well as throughout the Zhongba locality. Luminescence dating results for two ceramic sherds found on the surface at Zhongba 10-9b (1060 ± 160, UW2679 and 1330 ± 180 cal yr BP, UW2676) are similar to the uppermost age from this section (1310 ± 40 cal yr BP, 19-9b-4), supporting contemporaneity of human occupation with the final episode of wetlands formation.

Unit D: <2.0 ka BP

Unit D is the youngest unit in the study area, and likely dates to the last 2.0 ka. It is found only at Zhongba overlying Unit C, with a diachronous lower contact. It consists of loose, sterile, non-calcareous sand with eolian crossbedding and extensive root bioturbation. Sedimentologic or faunal evidence for wetlands is conspicuously absent, with the exception of two wetlands ages from Zhongba identifying a wet interval from 1.3 to 1.0 ka BP. Unit D, where found, likely represents drier-than-modern conditions, which allowed increased mobilization of eolian sand within the interdune deposits, and may be expressed only by the erosion of the depressions currently occupied by the modern interdune ponds at most sites. No artifacts have been found *in situ* within or clearly associated with this unit.

Paleoclimatic significance of paleowetlands deposits compared to regional records

The changing abundance, stratigraphic relationships, and facies composition of the paleowetlands deposits through time indicate significant environmental change in the upper YT valley spanning 10.4 ka BP to present. Overall, the four units represent a drying trend in the southwestern Tibetan Plateau since the early Holocene, recording decreasing intensity of the Indian Summer Monsoon (ISM). This drying trend is in good agreement with paleoclimate reconstructions from the Tibetan Plateau and Arabian Sea region (Figs. 8 and 9). Notably, even proxy records located in the northwest Himalaya (Tso Kar and Tso Moriri), which receives up to 50% winter precipitation today, show a nearly identical Holocene pattern of change in lake levels (Wünneman et al., 2009; Kramer et al., 2014) and vegetation change (Demske et al., 2009; Leipe et al., 2014) to those nearer to our study area (Ngangla Ring Tso; Hudson et al., 2015), indicating even these areas were most strongly affected by changing summer monsoon intensity during the early and mid-Holocene. Similarly, sediments from Qinghai Lake, located on the northeastern Tibetan Plateau, record the same general pattern in core proxies for monsoon-derived runoff (An et al., 2012), vegetation abundance (Shen et al., 2005; An et al., 2012), and lake depth (Lister et al., 1991), despite the fact that this location is affected by a mixture of Indian Summer Monsoon, East Asian Summer Monsoon and Westerly precipitation under modern conditions. Regardless of monsoon moisture source, it is clear that monsoon rainfall was enhanced relative to modern across the Tibetan Plateau during the early and mid-Holocene, and generally declined towards the present, coincident with high Northern Hemisphere summer insolation. For the purpose of describing the paleoclimate and prehistoric archaeological record of the Tibetan Plateau in more detail, it is convenient to compare select records during the early (ca. 11.7–8.0 cal ka BP), mid (ca. 8.0–4.0 cal ka BP) and late Holocene (ca. 4.0 cal ka BP to present) time intervals, which correspond well with the unit ages in this study.

The base of Unit A (ca. 10.4 to >8.0 ka BP) is not exposed in the study area, and so its basal age is unknown. Despite the limited exposure, Unit A indicates the presence of significant wet meadow deposits during the early Holocene at Zhongba, Tsangpo 18 and Tsangpo 20. Unit B (ca. 7.9–4.0 ka BP) is the most voluminous of the wetlands deposits, attesting to expansive wet meadows and marshes covering the valley floors in the interdune wetlands sites (Zhongba, Tsangpo 18, Yulai Cun), and perennial streamflow in now ephemeral drainages in the Kay Lak valley (KL 10-3, 13-3). The extensive soft sediment deformation structures within Unit B likely resulted from repeated freeze/thaw cycles within the saturated dune sands, indicating persistent widespread inundation of the interdune wetlands areas by the shallow water table. Together, Units A and B corroborate evidence of high lake levels in large closed-basin lake systems Ngangla Ring Tso (Hudson et al., 2015; Fig. 8), Baqan Tso (Huth et al., 2015), Tso Kar (Wünnemann et al., 2010), Tangra Yumco (Ahlborn et al., 2016), and Paiku Tso (Wünnemann et al., 2015), all indicating wettest conditions during the early Holocene with wetter-than-present conditions persisting throughout the mid-Holocene. Pollen-based vegetation reconstructions from cores from Tso Kar (Demske et al., 2009), and Tso Moriri (Leipe et al., 2014; Fig. 8) likewise indicate that enhanced monsoon precipitation resulted in increased plant cover and a shift towards more mesic plant communities relative to modern. Quantitative precipitation reconstructions based on pollen from Tso Moriri (Leipe et al., 2014) and from hydrologic budget modeling of Baqan Tso (Huth et al., 2015) indicate annual precipitation increases up to 50–100% greater than modern for the region during the early and mid-Holocene. Similarly, the index of summer monsoon intensity from Qinghai Lake, a combination of percent $CaCO_3$ and total organic carbon reflecting runoff and vegetation cover from the basin, indicates the highest and most variable conditions during the Unit A and B intervals (An et al., 2012; Fig. 8). The record of speleothem $\delta^{18}O$ values from Tianmen Cave in central Tibet do not overlap with the period of deposition of Unit A. However, they are lowest during the period immediately preceding Unit B, likely in response to enhanced monsoon precipitation in the south central Tibetan Plateau as well (Cai et al., 2012; Fig. 8). They then increase throughout the period of Unit B deposition. The lowest values in a speleothem record from the Oman margin (Qunf Cave, Fleitmann et al., 2003; Fig. 8) also occur during the early and mid-Holocene, indicating the strong monsoon conditions in the YT valley were similar to those recorded across the greater Asian Summer Monsoon region.

In Unit C (ca. 4.6 to 2.0 ka BP), the increase in calcareous marsh deposits and lack of sediment deformation structures in the interdune localities indicate wetlands retracted to isolated marshes and ponds, also evidenced by less voluminous deposits. This change in wetlands environment is coeval with evidence in other records of decline to near-modern monsoon intensity after during the late Holocene. Lake levels at Ngangla Ring Tso declined to <10 m above modern, indicating near modern annual precipitation (Fig. 8). The pollen-based precipitation reconstruction from Tso Moriri indicates near modern annual precipitation after 4.0 ka BP. Speleothem formation ceased in the Tianmen Cave record, indicating lower available moisture in central Tibet during the late Holocene. Deposition of Unit C ceases in the Kay Lak valley (KL 13-1), at Tsangpo 18, and in most sections at Zhongba (10-8, 10-11, 13-2) by 2.0 ka BP. This indicates widespread desiccation of wetlands in the upper YT valley after 2.0 ka BP, in agreement with lake levels declining to below modern at Ngangla Ring Tso. Likewise, near modern annual precipitation is indicated in the Tso Moriri pollen record for 3.0–1.0 ka BP.

The beginning of deposition of Unit D (ca. <2.0 ka BP to present) overlaps with the termination of C, depending on site. This non-calcareous, eolian unit suggests remobilization and deposition of dune sands in the interdune wetlands localities in response to dry climate. It is not directly dated, but persistent drier-than-modern

https://doi.org/10.1016/j.yqres.2016.04.001 Published online by Cambridge University Press

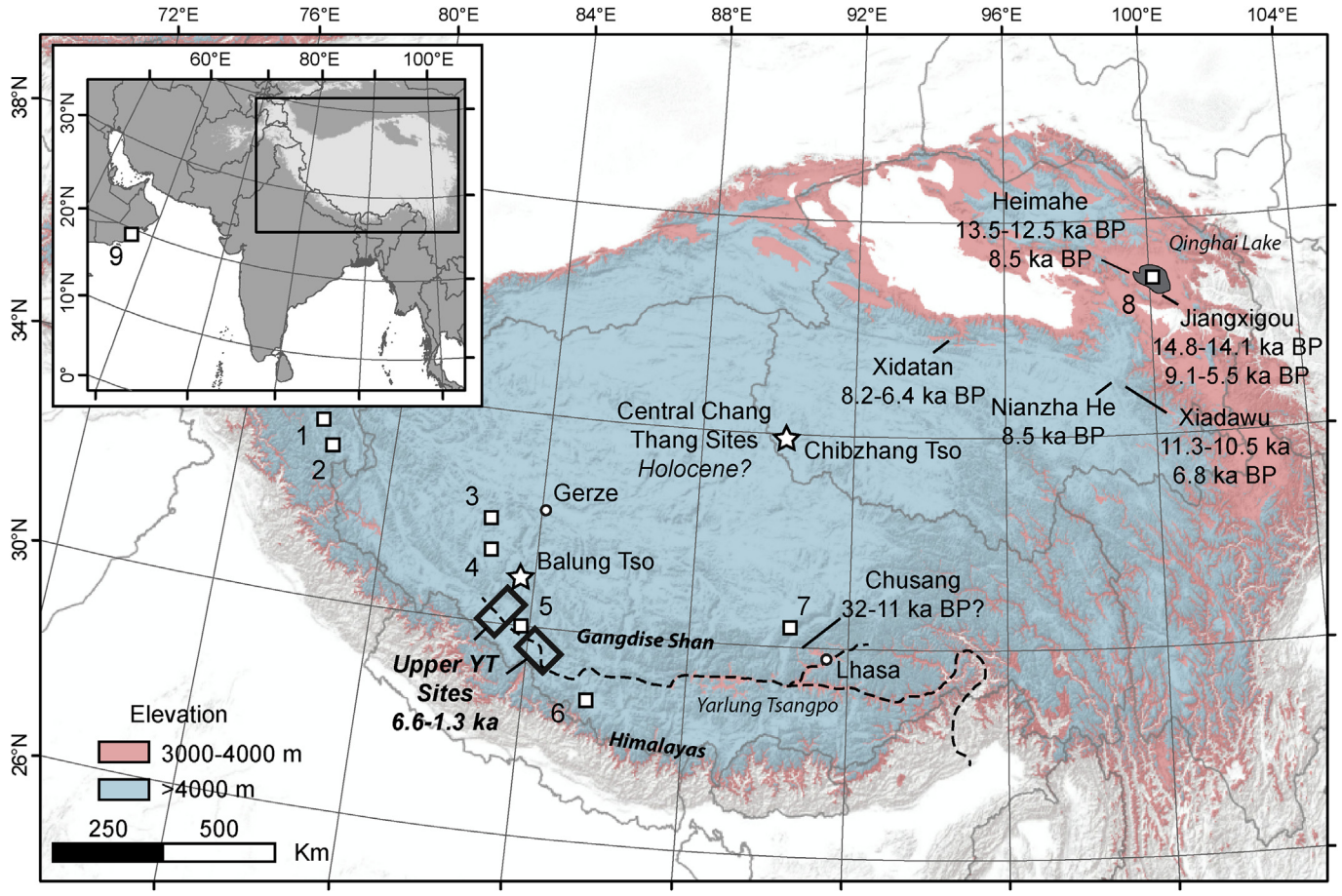

Figure 9. Tibetan Plateau paleoclimate records and prehistoric archaeological sites. Inset shows wider monsoon –influenced area with area of the Tibetan Plateau shown by the black box. Wetlands study areas are shown by black boxes labeled in bold with span of artifact-constraining ages. Paleoclimate records are shown by white squares; 1 – Tso Kar, Demske et al., 2009; Wünneman et al., 2010; 2 – Tso Moriri, Leipe et al., 2014; 3 – Baqan Tso, Huth et al., 2015; 4 – Ngangla Ring Tso, Hudson et al., 2015; 5 – Zhuzhu dune/paleosol section, Li et al., 2016; 6 –Paiku Tso, Wünnemann et al., 2015; 7 – Tianmen Cave, Cai et al., 2012; 8 – Qinghai Lake, An et al., 2012; 9 – Qunf Cave, Fleitmann et al., 2003. Archaeological sites are labeled by name and span of ages; Xidatan – Brantingham et al., 2013; Heimahe, Jiangxigou, Madsen et al., 2007; Rhode et al., 2006; Nianzha He/Xiadawu – Van Der Woerd et al., 2002; Central Chang Thang sites, An, 1982; Brantingham et al., 2001; Aldenderfer and Zhang, 2004; Chusang – Aldenderfer and Zhang, 2004; Zhang and Li, 2002; Rhode, 2016. Age spans indicate only the full range of available ages, not continuous occupation of the sites. Sites with significant age uncertainty are denoted by question marks. Known archaeological obsidian sources are shown by white stars (Perreault et al., 2016). Land area between 3000 and 4000 m elevation shown in pink, >4000 m elevation in light blue. (For interpretation of the references to colour in this figure legend, the reader is referred to the web version of this article.)

conditions are indicated by Ngangla Ring Tso lake level below modern, consistent with Unit D being largely deposited during a period of monsoon drought in the southwestern Tibetan Plateau. A minor wet episode recorded by pond marls and thin black mats of 1.3–1.0 ka BP age at Zhongba indicates wetlands were scarce, but existent, even during this dry interval.

In addition to the paleohydrologic evidence from the four major lithostratigraphic units at the millennial scale, the ^{14}C dating results and sedimentary unconformities indicate coeval periods of enhanced wetlands formation, and desiccation and deflation at the centennial scale across all localities (Figs. 7 and 8). In Unit A, the period of wetlands formation at 10.4 ka and 9.6 ka BP corresponds to the highest inferred monsoon intensity in the speleothem records, and prominent peaks in the Tso Moriri precipitation reconstruction, the Qinghai Lake monsoon index, and the highest lake level at Ngangla Ring Tso. Similarly, the lack of wetlands between 9.6 and 8.0 ka BP, which forms the unconformable lower boundary of Unit B, corresponds broadly to the '8.2 ka' weak monsoon event noted in the speleothem records and lake level regression at Ngangla Ring Tso. Variable, but generally wet conditions, persist in all records during the period of deposition of Unit B (ca. 7.9–4.8 ka BP), in agreement with the wide occurrence and variable sedimentary makeup of this wetlands unit in the study area. Within this period, wetlands ages from 7.9 to 7.4 ka BP are consistent with a ^{14}C-dated paleosol at ~7.6 ka BP, indicating dune stabilization in an eolian sediment sequence at Zhuzhu between the Zhongba and Tsangpo localities (Li et al., 2016; Fig. 8). Following this wet period, a dramatic regression in Ngangla Ring Tso lake level at 6.0 ka BP is consistent with an absence of wetlands ages from 6.5 to 5.5 ka BP, indicating a dry interval in the study area. A following lake level high interval from 5.5 to 4.0 ka BP is coeval with ample wetlands ^{14}C ages, though it spans the unconformable boundary between Units B and C. Finally, the later period of deposition of Unit C (ca. 2.7–2.0 ka BP) is coeval with paleosol development in the Zhuzhu section from 3.3 to 2.5 ka BP, a final near modern highstand in Ngangla Ring Tso and near-modern precipitation conditions inferred from Tso Moriri. The occurrence of minor wetlands from 1.3 to 1.0 ka BP, similar to the uppermost paleosol age from the Zhuzhu section of 0.8 ka BP, indicate a final wet period in the late Holocene superimposed upon drier than modern conditions by Ngangla Ring Tso lake levels.

Overall the record of wetlands formation in the upper YT valley provides additional evidence for significant monsoon intensification across the whole Tibetan Plateau in response to increased

https://doi.org/10.1016/j.yqres.2016.04.001 Published online by Cambridge University Press

Northern Hemisphere summer insolation during the early Holocene, declining through the mid Holocene and similar to or lower than modern during the late Holocene. This overall trend was punctuated by regionally coherent strong and weak monsoon events at the centennial scale, which resulted in large and persistent hydrological changes.

Paleowetlands archaeological record

The paleowetlands deposits in the upper YT valley are commonly associated with *in situ* or adjacent surface collections of lithic and ceramic artifacts. This association indicates the presence of prehistoric people utilizing the YT wetlands in the southwestern Tibetan Plateau during the mid and late Holocene. Artifacts found *in situ* in Units B and C within the stratigraphic sections provide a rare opportunity to constrain the age of human occupation. Artifacts have been previously found *in situ* within Unit B at Zhongba 10-1, and in Unit C at Zhongba 10-9b and are constrained in age to 6.6–2.6 ka BP and 3.4–1.3 ka BP, respectively (Fig. 4; Hudson et al., 2014). Additional *in situ* artifacts at Kay Lak 10-3, and Yulai Cun 13-1 (Figs. 5 and 10), both in Unit B, provide further evidence for human occupation of mid Holocene age.

The artifact at Kay Lak 10-3, a single typologically-indistinct obsidian flake (Fig. 10A), is constrained by a humate minimum age of 6550 ± 90 cal yr BP (10-3-1). This age is similar to the lower age bound of the time interval indicated for lithic artifacts at site Zhongba 10-1, suggesting human occupation of the region has occurred since at least 6.6 ka BP. This obsidian flake has been identified by X-ray Fluorescence (XRF) trace element analysis as being sourced locally from cobbles on the shore of Balung Tso located 27 km to the north of the Kay Lak valley (Southwestern Obsidian D; Perreault et al., 2016).

Two *in situ* ceramic sherds found at Yulai Cun 13-1 (Fig. 10B) are constrained by humate minimum ages above and below the artifacts to an age range of 5.2–4.8 ka BP (YLC13-1-1H, YLC13-1-5H). This age is significantly older than the luminescence ages determined for ceramic sherds from Zhongba 10-9b (1060 ± 80 yr and 1390 ± 80 yr BP), indicating ceramics were also being used as early as the mid-Holocene. The appearance of archaeological materials during the deposition of Unit B in the upper YT valley suggests prehistoric populations occupied the region by 6.6 ka BP when paleoclimate records indicate 40–100% greater Indian Summer Monsoon precipitation relative to modern (Leipe et al., 2014; Huth et al., 2015). The paleowetlands record attests to increased availability of surface water, and increased vegetation cover, which likely facilitated human occupation in the study area, as it still does for the modern settlements and nomadic herders.

Relationship of YT localities to regional archaeological sites

Relating human occupation of the upper YT valley during the Holocene to archaeological sites elsewhere on the Tibetan Plateau is challenging. The small assemblages of mostly lithic artifacts that characterize most plateau sites provide little information about human behavior that can be used to define a 'cultural tradition' between prehistoric people. The main criterion for relating and grouping sites has focused on recurring types of lithic artifacts that suggest a shared method for the production of stone tools (e.g. Brantingham and Gao, 2006). This has been supplemented recently by trace element provenance analysis of obsidian artifacts from sites in the northeastern and southwestern Tibetan Plateau, including the Zhongba and Kay Lak valley localities from this study (Perreault et al., 2016). The majority of lithic assemblages in Tibetan Plateau sites are microlithic, characterized by small (mm to cm scale) rectangular blades and associated cores and debitage produced on very fine-grained lithologies like quartzite, chert, obsidian, and other volcanic rocks (Fig. 10). The most diagnostic artifact types are the blades themselves and the wedge-shaped or conical "bullet" cores from which they were flaked (Fig 10D). Large discoidal prepared cores used for producing tablet-shaped flakes (Fig. 10C) are also diagnostic (Brantingham and Gao, 2006). Microblades and all three core types are common in the upper YT assemblages, which supports grouping them with sites exhibiting the Epipaleolithic microlith toolkit that is found widely across the high Tibetan Plateau and the Qinghai Lake region (Fig. 9). However, the provenance of obsidian artifacts indicates that it is too simplistic to consider them a single prehistoric population. Perreault et al. (2016) identified five types of archaeological obsidian by XRF. Two types, Northeastern Osibidian A and B, are found only in sites in the Chang Thang region and near Qinghai Lake and are likely derived from different lava flows of the same volcanic source near the lake Chibzhang Tso (Fig. 9). Northeastern Obsidian C is found in only one site in the central Chang Thang with an unknown source. The other two types are found only in sites in the upper YT valley and directly adjacent regions of the southwestern Tibetan Plateau. The geologic source of Southwest Obsidian B is local to the Kay Lak valley localities near the lake Balung Tso (Fig. 9). The geologic provenance of Southwest Obsidian A is unknown, but it is widespread in archaeological sites along the upper YT valley (e.g. Zhongba, Kay Lak 13-3), and near the shores of Ngangla Ring Tso to the north, and Paiku Tso to the south of the YT. With inferred transport distances of 100's of km from the geologic sources, these obsidian artifacts indicate prehistoric Tibetan populations were highly mobile, but clearly separate northeastern and southwestern zones of lithic transport. Significant additional work is needed to assess whether this separation is due to separate populations employing the same microlithic toolkit, or the propensity/need to exploit the most local geologic sources of raw material.

Paleoclimate and the colonization history of the Tibetan Plateau

Although much of the archaeological record of the plateau is found in surface collections, an increasing number of localities, including those in this study, have sufficient age control to make age comparisons at the regional scale, and human influence on the landscape has also been dated indirectly using paleoenvironmental proxies. This evidence provides a rough approximation of the sequence and extent of human occupation of the middle elevations (3000–4000 m asl) during the late glacial and the high Tibetan Plateau (>4000 m asl) during the Holocene, which underpins the main hypothesis for plateau colonization (Fig. 9).

There is currently very limited evidence for human occupation on the high Tibetan Plateau prior to the Holocene. A single site from the central plateau, Chusang, consisting of a hearth feature and human hand and footprints in spring travertine, has been inconsistently dated perhaps to the last glacial maximum or older (Aldenderfer and Zhang, 2004). Zhang and Li (2002) determined an age of ~21 ka BP by OSL dating of detrital eolian quartz in the travertine of the hearth and prints, while U-series ages of ~28–32 ka BP were obtained for the travertine underlying the prints under the assumption that they were pressed into carbonate mud of similar age (Aldenderfer and Zhang, 2004). An early Holocene charcoal age from the hearth of ~11 ka BP has also been alluded to, but never formally published (Brantingham et al., 2007; Rhode, 2016). The vast difference in age between the site components is difficult to explain and more work is required to reconcile the age of this site.

The next oldest securely dated sites on the Tibetan Plateau come from 3000–4000 asl in the Qinghai Lake basin in the

https://doi.org/10.1016/j.yqres.2016.04.001 Published online by Cambridge University Press

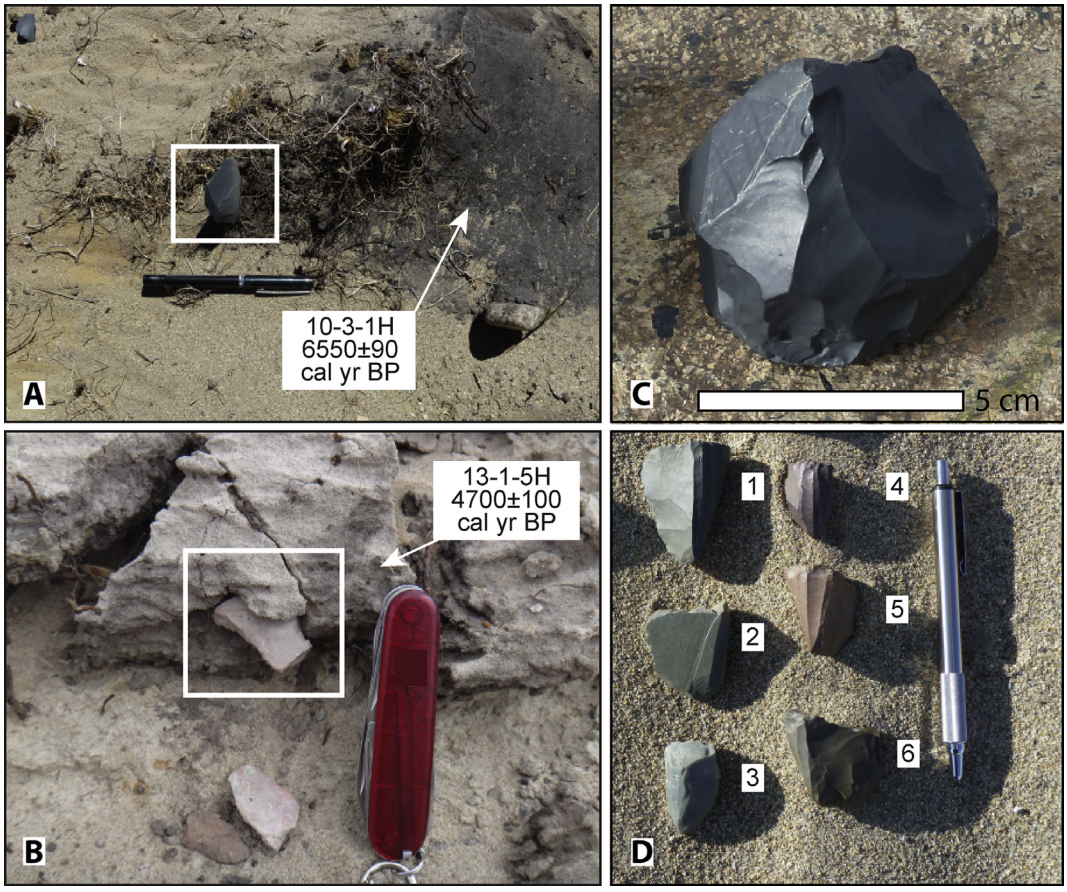

Figure 10. Photographs of artifacts from paleowetlands sites. Artifact locations are indicated by white boxes. Constraining ^{14}C samples and ages are indicated by white arrows. A – obsidian flake, KL10-3 site, central Kay Lak valley. Pen for scale is 15 cm in length. Photo credit: A. Hudson, June 18, 2010. B – redware ceramic sherds, YLC13-1 site, Yulai Cun locality. Knife for scale is 9 cm in length. Photo credit: A. Hudson, June 18, 2013. C – chert discoidal prepared core, Zhongba site. Photo credit: J. Olsen, June 16, 2010. D – wedge-shaped (1, 2, 5, 6) and conical (3, 4) microblade cores, Zhongba site. Pen for scale is 14 cm in length. Photo credit: J. Olsen, June 17, 2010.

northeast (Fig. 9). The stratified Jiangxigou and Heimahe sites contain horizons with *in situ* artifacts and constraining hearth charcoal ages of 14.8–12.5 ka BP (Madsen et al., 2006), unequivocally indicating the presence of hunter/foragers at middle elevation during the colder, drier climate conditions of the Late Glacial period (ca. 18.0–11.7 ka BP). The artifact assemblages of Late Glacial age differ significantly from the Holocene microlithic package, being aceramic and based on larger flake and blade tools, although some microblades were found (Madsen et al., 2006). True microblade assemblages are known from the lowland areas of Gansu province adjacent to the plateau during the late glacial as well (e.g. Yi et al., 2013). Hunter/foragers using the late glacial toolkit at Heimahe were still apparently present during the early Holocene, constrained by a charcoal age of 8.5 ka BP (Rhode et al., 2006). However, Jiangxigou nearby was occupied during the early and middle Holocene (9.1–5.5 ka BP) by inhabitants using pottery and microliths similar to those found in the upper YT valley (Rhode et al., 2007; Rhode, 2016). Archaeological sites with microlithic assemblages also begin to appear on the high interior of the plateau (>4000 m asl) during the early and mid Holocene. Microlithic artifacts have been dated to 8.2–6.4 ka BP in a high elevation site, Xidatan (Fig. 8), located in Kunlun Mountains of the northeastern Tibetan Plateau (Brantingham and Gao, 2006; Brantingham et al., 2013) and archaeological charcoal associated with microliths in river terrace deposits has been dated to ~8.5 ka BP at Nianzha He (4100 m asl) and as early 11.3 ka BP at Xiadawu (4000 m asl) southwest of Qinghai Lake (Van Der Woerd et al., 2002; Rhode, 2016). Numerous undated open-air sites with similar artifact typology have been assigned Holocene age in the Chang Thang region of the central Tibetan Plateau near to the purported source of Northwest Obsidians A and B (An, 1982; Brantingham et al., 2001). Previous researchers (e.g. Brantingham and Gao, 2006; Rhode, 2016) regard this microlithic toolkit as indicating highly mobile hunting/foraging groups subsisting on the widely varied herbivorous game species of the Tibetan Plateau. The persistence of this toolkit virtually unchanged in the southwestern sites studied here during the mid- and late Holocene may therefore indicate this mobile hunting adaptation allowed people to colonize the plateau from the northeast under the favorable climate conditions of the early and mid-Holocene, and persist until relatively recent times.

However, significant indirect paleoenvironmental information also indicates widespread human presence on the high plateau by the mid-Holocene consistent with a pastoralist adaptation. Palynological evidence for anthropogenic forest replacement by grasslands favorable for livestock grazing during the mid-Holocene has been noted on the high plateau margins in the northeastern Tibetan Plateau and the northwest Himalaya by ~8.1 and 5.7 ka BP, respectively (Miehe et al., 2008, 2009, 2014). Enhanced slope erosion in the eastern reaches of the YT valley by ~7.0 ka BP (Pelletier et al., 2011), and anthropogenic burn layers in valley fill deposits of northern Bhutan at 6.7 ka BP (Meyer et al., 2009) are also likely connected to human land use and management for grazing. The sum of this evidence indirectly indicates pastoralism

https://doi.org/10.1016/j.yqres.2016.04.001 Published online by Cambridge University Press

may have also been an important subsistence strategy for mid-Holocene populations.

In any case, the current dearth of artifacts and archaeo-faunal evidence directly pointing to hunting/foraging or pastoralism in plateau archaeological sites leaves the debate over primary subsistence strategy in need of further research. It is currently unclear whether the widely-occurring microlithic toolkit was employed by hunter/foragers, pastoralists, or both. The wide distribution of archaeological sites and indirect environmental evidence do however indicate widespread occupation of the high Tibetan Plateau (>4000 m asl) starting in the northeastern plateau during the early Holocene and appearing across the plateau in the upper YT valley by the mid-Holocene, coincident with significantly warmer, wetter climate conditions relative to the preceding late glacial period. The clear existence of a similar microlithic toolkit in adjacent lowland areas prior to the Holocene (Yi et al., 2013) suggests development of this strategy was not sufficient to colonize the high plateau alone. Enhanced monsoon conditions expanding vegetation on the Tibetan Plateau would have benefited populations of wild or domestic grazing animals, ultimately facilitating movement of humans practicing either hunting/foraging or pastoralism, or both, onto the highest area of the planet on a more permanent basis. Competitive exclusion of these highly mobile populations from lowland areas by incipient sedentary agriculturalists like the Yangshao culture may have provided additional impetus to move to greener early Holocene pastures (Brantingham et al., 2007). While our work adds to the rapidly evolving story of human colonization, much of the vast high Tibetan Plateau remains poorly studied and more work is still required to understand the likely complex history of human occupation.

Conclusions

^{14}C dating of black mats in this study highlights the problems that contamination from modern roots and younger organic material can pose when dating bulk organic matter in wetlands deposits. Dating of thirteen residue/humate fraction pairs indicates that the insoluble residue fraction provides the most reliable ages in most cases, because younger soluble humate material often contaminates the primary organics, causing anomalous younging of humate ages. However, some humate ages were indistinguishable from the insoluble residues where not overlain by younger organics, and humate ages were older than residues in black mats with extensive root contamination, indicating humate dating may provide more reliable ages where roots cannot be fully eliminated. The results of this dating experiment allowed us to pick the most reliable ages for the paleowetlands sediments, providing a chronostratigraphic framework for wetlands formation in the YT valley since 10.4 ka BP. The history of wetlands deposition in the Yarlung Tsangpo valley provides a novel record of hydrologic variability related to changing summer monsoon intensity in the southern Tibetan Plateau. In agreement with other regional paleoclimate records, the four stratigraphic units A-D record declining wetlands extent and vegetation abundance as monsoon rainfall waned since ca. 9.6 ka BP. Overlapping ^{14}C ages from multiple wetlands sites distributed along the YT valley indicate wet monsoon periods at ca. 10.4, 9.6, 7.9–7.4, 6.6, 5.2–4.1, 3.4, 2.7–2.0 and 1.3–1.0 ka BP, while erosional periods marking unit boundaries indicate dry periods at ca. 8.0 ka BP, 6.5–5.5 ka BP, 4.8 ka BP, 4.0–3.5 ka, 2.0–1.4 ka BP, and 1.0 ka BP to present. *In situ* lithic and ceramic artifacts in two sites are constrained to ~6.6 and 5.2–4.8 ka BP. Two additional ceramics yield luminescence ages of ~1.2 ka BP. These age constraints on human occupation in the southwestern Tibetan Plateau add to increasing evidence for widespread colonization of regions >4000 m asl during the early and mid-Holocene, facilitated by warm, wet climate conditions.

Acknowledgments

This research was funded by grants from the Henry Luce Foundation, the American Council of Learned Societies, the Comer Science and Education Foundation, and the University of Arizona Je Tsongkhapa Endowment for Central and Inner Asian Archaeology. We thank Nyingcha-gyal, John Pelletier, and Erin Clair for assistance in the field, Marie de los Santos for assistance with laboratory preparation, and James Feathers for providing OSL measurements and assistance with the OSL methods. We also thank Jeff Pigati and two anonymous reviewers whose comments greatly improved this work.

References

Adamiec, G., Aitken, M.J., 1998. Dose rate conversion factors: update. Ancient TL 16, 37–50.
Ahlborn, M., Haberzettl, T., Wang, J., Fürstenberg, S., Mäusbacher, R., Mazzoco, J., Pierson, J., Zhu, L., Frenzel, P., 2016. Holocene lake level history of the Tangra Yumco lake system, southern-central Tibetan Plateau. The Holocene 26, 176–187.
Aldenderfer, M., Zhang, Y., 2004. The prehistory of the Tibetan Plateau to the seventh century A.D.: perspectives and research from China and west since 1950. Journal of World Prehistory 18, 1–55.
An, Z., 1982. Palaeoliths and microliths from Shena and Shuanghu, northern Tibet. Current Anthropology 23, 493–499.
An, Z., Colman, S.M., Zhou, W., Li, X., Brown, E.T., Jull, A.J.T., Cai, Y., Huang, Y., Chang, H., Song, Y., Sun, Y., Xu, H., Liu, W., Jin, Z., Liu, X., Cheng, P., Liu, Y., Ai, L., Li, X., Liu, X., Yan, L., Shi, Z., Wang, X., Wu, F., Qiang, X., Dong, J., Lu, F., Xu, X., 2012. Interplay between the Westerlies and Asian monsoon recorded in Lake Qinghai sediments since 32 ka. Nature Scientific Reports 2. http://dx.doi.org/10.1038/srep00619.
Andermann, C., Longuevergne, L., Bonnet, S., Crave, A., Davy, P., Gloaguen, R., 2012. Impact of transient groundwater storage on the discharge of Himalayan rivers. Nature Geoscience 5, 127–132.
Ashley, G.M., Tactikos, J.C., Owen, R.B., 2009. Hominin use of springs and wetlands: Paleoclimate archaeological records from Olduvai Gorge (~1.79-1.74 Ma). Palaeogeography, Palaeoclimatology, Palaeoecology 272, 1–16.
Banerjee, D., Murray, A.S., Bøtter-Jensen, L., Lang, A., 2001. Equivalent dose estimation using a single aliquot of polymineral fine grains. Radiation Measurements 33, 73–93.
Berger, A., Loutre, M.F., 1991. Insolation values for the climate of the last 10 million years. Quaternary Science Reviews 10, 297–317.
Betancourt, J.L., Latorre, C., Rech, J.A., Quade, J., Rylander, K.A., 2000. A 22,000-year record of monsoonal precipitation from northern Chile's Atacama Desert. Science 289, 1542–1546.
Bleicher, N., 2013. Summed radiocarbon probability density functions cannot prove solar forcing of Central European lake-level changes. The Holocene 23, 755–765.
Bookhagen, B., Burbank, D.W., 2010. Towards a complete Himalayan hydrological budget: spatiotemporal distribution of snowmelt and rainfall and their impact on river discharge. Journal of Geophysical Research 115, F03019. http://dx.doi.org/10.1029/2009JF001426.
Brantingham, P.J., Olsen, J.W., Schaller, G., 2001. Lithic assemblages from the Chang Tang region, northern Tibet. Antiquity 75, 319–327.
Brantingham, P.J., Gao, X., 2006. Peopling of the northern Tibetan Plateau. World Archaeology 38, 387–414.
Brantingham, P.J., Xing, G., Olsen, J.W., Ma, H., Rhode, D., Zhang, H., Madsen, D.B., 2007. A short chronology for the peopling of the Tibetan Plateau. Developments in Quaternary Sciences 9, 129–150.
Brantingham, P.J., Gao, X., Madsen, D.B., Rhode, D., Perreault, C., van der Woerd, J., Olsen, J.W., 2013. Late occupation of the high-elevation northern Tibetan Plateau based on cosmogenic, luminescence, and radiocarbon ages. Geoarchaeology 28, 413–431.
Bronk Ramsey, C., 2009. Bayesian analysis of radiocarbon dates. Radiocarbon 51, 337–360.
Cai, Y., Zhang, H., Cheng, H., An, Z., Edwards, R.L., Wang, X., Tan, L., Liang, F., Wang, J., Kelly, M., 2012. The Holocene Indian monsoon variability over the southern Tibetan Plateau and its teleconnections. Earth and Planetary Science Letters 335, 135–144.
Carrapa, B., Orme, D.A., DeCelles, P.G., Kapp, P., Cosca, M.A., Waldrip, R., 2015. Miocene burial and exhumation of the India-Asia collision zone in southern Tibet: response to slab dynamics and erosion. Geology 42, 443–446.
Deines, P., 1980. The isotopic composition of reduced organic carbon. In: Fritz, P., Fontes, J.C. (Eds.), Handbook of Environmental Isotope Geochemistry, The Terrestrial Environment A, vol. 1. Elsevier, Amsterdam, pp. 23–406.

Demske, D., Tarasov, P.E., Wünneman, B., Riedel, F., 2009. Late glacial and Holocene vegetation, Indian monsoon and westerly circulation in the Trans-Himalaya recorded in the lacustrine pollen sequence from Tso Kar, Ladakh, NW India. Palaeogeography, Palaeoclimatology, Palaeoecology 279, 172–185.

Ding, L., Kapp, P., Wan, X., 2005. Paleocene-Eocene record of ophiolite obduction and initial India-Asia collision, south central Tibet. Tectonics 24. http://dx.doi.org/10.1029/2004TC001729.

Feathers, J.K., 2009. Problems of ceramic chronology in the Southeast: does shell-tempered pottery appear earlier than we think? American Antiquity 74, 113–142.

Fleitmann, D., Burns, S.J., Mudelsee, M., Neff, U., Kramers, J., Mangini, A., Matter, A., 2003. Holocene forcing of the Indian monsoon recorded in a stalagmite from southern Oman. Science 300, 1737–1739.

Harris-Parks, E., 2016. The micromorphology of Younger Dryas-aged black mats from Nevada, Arizona, Texas and New Mexico. Quaternary Research 85, 94–106. http://dx.doi.org/10.1016/j.yqres2015.11.005.

Haynes Jr., C.V., 2008. Younger Dryas "black mats" and the Rancholabrean termination in North America. Proceedings of the National Academy of Sciences 105, 6520–6525.

Hou, J., D'Andrea, W.J., Liu, Z., 2012. The influence of ^{14}C reservoir age on interpretation of paleolimnological records from the Tibetan Plateau. Quaternary Science Reviews 48, 67–79.

Hudson, A.M., Quade, J., Huth, T.E., Lei, G., Cheng, H., Edwards, R.L., Olsen, J.W., Zhang, H., 2015. Lake level reconstruction for 12.8-2.3 ka for the Ngangla Ring Tso closed-basin lake system, southwest Tibetan Plateau. Quaternary Research 83, 66–79.

Hudson, A.M., Olsen, J.W., Quade, J., 2014. Radiocarbon dating of interdune paleowetland deposits to constrain the age of mid-to-Late Holocene microlithic artifacts from the Zhongba site, southwestern Qinghai-Tibet Plateau. Geoarchaeology 29, 33–46.

Hudson, A.M., Quade, J., 2013. Long-term east-west asymmetry in monsoon rainfall on the Tibetan Plateau. Geology 41, 351–354.

Huth, T.E., Hudson, A.M., Quade, J., Lei, G., Zhang, H., 2015. Paleohydrologic reconstruction of Holocene climate 11.5-5.0 ka based on shoreline dating and hydrologic budget modeling of Baqan Tso, southwestern Tibetan Plateau. Quaternary Research 83, 80–93.

Kong, P., Na, C., Fink, D., Huang, F., Ding, L., 2007. Cosmogenic ^{10}Be inferred lake-level changes in Sumxi Co basin, western Tibet. Journal of Asian Earth Sciences 29, 698–703.

Kramer, M., Kotlia, B.S., Wünneman, B., 2014. A late Quaternary ostracod record from the Tso Kar basin (North India) with a note on distribution of recent species. Paleolimnology 51, 549–565.

Kummerow, C., Barnes, W., Kozu, T., Shiue, J., Simpson, J., 1998. The Tropical Rainfall Measuring Mission (TRMM) sensor package. Journal of Atmospheric and Oceanic Technology 15, 809–817.

Leipe, C., Demske, D., Tarasov, P.E., HIMPAC Project Members, 2014. A Holocene pollen record from the northwestern Himalayan lake Tso Moriri: implications for palaeoclimatic and archaeological research. Quaternary International 348, 93–112.

Lee, J., Li, S., Aitchison, J.C., 2009. OSL dating of paleoshorelines at Lagkor Tso, western Tibet. Quaternary Geochronology 4, 335–343.

Li, Q., Lu, H., Zhu, L., Wu, N., Wang, J., Lu, X., 2011. Pollen-inferred climate changes and vertical shifts of alpine vegetation belts on the northern slope of the Nyainqentanglha Mountains (central Tibetan Plateau) since 8.4 kyr BP. The Holocene 21, 939–950.

Li, T., Wu, Y., Du, S., Huang, W., Hao, C., Guo, C., Zhang, M., Fu, T., 2016. Geochemical characterization of a Holocene aeolian profile in the Zhongba area (southern Tibet, China) and its paleoclimatic implications. Aeolian Research 20, 169–175.

Lister, G.S., Kelts, K., Zao, C.K., Yu, J., Niessen, F., 1991. Lake Qinghai, China: closed-basin lake levels and the oxygen isotope record for ostracoda since the latest Pleistocene. Palaeogeography, Palaeoclimatology. Palaeoecology 84, 141–162.

Liu, X.J., Lai, Z.P., Zeng, F.M., Madsen, D.B., Chong, Y.E., 2013. Holocene lake level variations on the Qinghai-Tibet Plateau. International Journal of Earth Sciences 102, 2007–2016.

Liu, K.B., Yao, Z., Thompson, L.G., 1998. A pollen record of Holocene climatic changes from the Dunde ice cap, Qinghai-Tibetan Plateau. Geology 26, 135–138.

Madsen, D.B., Ma, H., Brantingham, P.J., Gao, X., Rhode, D., Zhang, H., Olsen, J.W., 2006. The late Upper Paleolithic occupation of the northern Tibetan Plateau margin. Journal of Archaeological Science 33, 1433–1444.

Meyer, M.C., Hofmann, Ch.-Ch., Gemmell, A.M.D., Haslinger, E., Häusler, H., Wangda, D., 2009. Holocene glacier fluctuations and migration of Neolithic yak pastoralists into the high valleys of northwest Bhutan. Quaternary Science Reviews 28, 1217–1237.

Miehe, G., Kaiser, K., Co, S., Zhao, X., Liu, J., 2008. Geo-ecological transect studies in northeast Tibet (Qinghai, China) reveal human-made mid-Holocene environmental changes in the upper Yellow River catchment changing forest to grassland. Erdkunde 62, 187–199.

Miehe, G., Miehe, S., Schlütz, F., 2009. Early human impact in the forest ecotone of southern High Asia (Hindu Kush, Himalaya). Quaternary Research 71, 255–265.

Miehe, G., Miehe, S., Bohner, J., Kaiser, K., Hensen, I., Madsen, D., Liu, J.Q., Opgenoorth, L., 2014. How old is the human footprint in the world's largest alpine ecosystem? A review of multiproxy records from the Tibetan Plateau from the ecologists' viewpoint. Quaternary Science Reviews 86, 190–209.

Mügler, I., Gleixner, G., Gunther, F., Mäusbacher, R., Daut, G., Schütt, B., Berking, J., Schwalb, A., Schwark, L., Xu, B., Yao, T., Zhu, L., Yi, C., 2010. A multi-proxy approach to reconstruct hydrological changes and Holocene climate development of Nam Co, central Tibet. Journal of Paleolimnology 43, 625–648.

Murray, A.S., Wintle, A.G., 2000. Luminescence dating of quartz using an improved single-aliquot regenerative-dose protocol. Radiation Measurements 32, 57–73.

Pan, B., Yi, C., Jiang, T., Dong, G., Hu, G., Jin, Y., 2012. Holocene lake-level changes of Linggo Co in central Tibet. Quaternary Geochronology 10, 117–122.

Pelletier, J.D., Quade, J., Goble, R.J., Aldenderfer, M.S., 2011. Widespread hillslope gullying on the southeastern Tibetan Plateau: human or climate-change induced? Geological Society of America Bulletin 123, 1926–1938.

Perreault, C., Boulanger, M.T., Hudson, A.M., Rhode, D., Madsen, D.B., Olsen, J.W., Steffen, M.L., Quade, J., Glascock, M.D., Brantingham, P.J., 2016. Characterization of obsidian from the Tibetan Plateau by XRF and NAA. Journal of Archaeological Science: Reports 5, 392–399.

Pigati, J.S., Quade, J., Shanahan, T.M., Haynes Jr., C.V., 2004. Radiocarbon dating of minute gastropods and new constraints on the timing of late Quaternary spring-discharge deposits in southern Arizona, USA. Palaeogeography, Palaeoclimatology, Palaeoecology 204, 33–45.

Pigati, J.S., Miller, D.M., Bright, J.E., Mahan, S.A., Nekola, J.C., Paces, J.B., 2011. Chronology, sedimentology, and microfauna of groundwater discharge deposits in the central Mojave Desert, Valley Wells, California. Geological Society of America Bulletin 123, 2224–2239.

Pigati, J.S., Rech, J.A., Quade, J., Bright, J., 2014. Desert wetlands in the geologic record. Earth-Science Reviews 132, 67–81.

Quade, J., Forester, R.M., Pratt, W.L., Carter, C., 1998. Black mats, spring-fed streams, and Late-Glacial-age recharge in the southern Great Basin. Quaternary Research 49, 129–148.

Quade, J., Rech, J.A., Betancourt, J.L., Latorre, C., Quade, B., Ryslander, K.A., Fisher, T., 2008. Paleowetlands and regional climate change in the central Atacama Desert, northern Chile. Quaternary Research 69, 343–360.

Rech, J.A., Pigati, J.S., Quade, J., Betancourt, J.L., 2003. Re-evaluation of mid-Holocene deposits at Quebrada Puripica, northern Chile. Palaeogeography, Palaeoclimatology, Palaeoecology 194, 207–222.

Reimer, P.J., Bard, E., Bayliss, A., Beck, J.W., Blackwell, P.G., Bronk Ramsey, C., Grootes, P.M., Guilderson, T.P., Haflidason, H., Hajdas, I., Hatt, C., Heaton, T.J., Hoffmann, D.L., Hogg, A.G., Hughen, K.A., Kaiser, K.F., Kromer, B., Manning, S.W., Niu, M., Reimer, R.W., Richards, D.A., Scott, E.M., Southon, J.R., Staff, R.A., Turney, C.S.M., van der Plicht, J., 2013. IntCal13 and Marine13 radiocarbon age calibration curves 0-50,000 years cal BP. Radiocarbon 55, 1869–1887.

Rhode, D., Zhang, H., Madsen, D.B., Gao, X., Brantingham, P.J., Ma, H., Olsen, J.W., 2007. Epipaleolithic/early Neolithic settlements at Qinghai Lake, western China. Journal of Archaeological Science 34, 600–612.

Rhode, D., 2016. A biogeographic perspective on early human colonization of the Tibetan Plateau. Archaeological Research in Asia. http://dx.doi.org/10.1016/j.ara.2016.01.004.

Roberts, H.M., Wintle, A.G., 2001. Equivalent dose determinations for polymineralic fine-grains using the SAR protocol: application to a Holocene sequence of the Chinese Loess Plateau. Quaternary Science Reviews 20, 859–863.

Shen, J., Liu, X., Wang, S., Ryo, M., 2005. Palaeoclimatic changes in the Qinghai Lake area during the last 18,000 years. Quaternary International 136, 131–140.

Slota, J.R., Jull, A.J.T., Linick, T.W., Toolin, L.J., 1987. Preparation of small samples for ^{14}C accelerator targets by catalytic reduction of CO. Radiocarbon 29, 303–306.

Springer, K.B., Manker, C.R., Pigati, J.S., 2015. Dynamic response of desert wetlands to abrupt climate change. Proceedings of the National Academy of Sciences 112, 14522–14526.

Styron, R.H., Taylor, M.H., Sundell, K.E., Stockli, D.F., Oalmann, J.A.G., McAllister, A.T., Liu, D., Ding, L., 2013. Miocene initiation and acceleration of extension in the South Lunggar rift, western Tibet: evolution of an active detachment system from structural mapping and (U-Th)/He thermochronology. Tectonics 32. http://dx.doi.org/10.1002/tect.20053.

Sun, Y., Lai, Z., Long, H., Liu, X., Fan, Q., 2010. Quartz OSL dating of archaeological sites in Xiao Qaidam Lake of the NE Qinghai–Tibetan Plateau and its implications for palaeoenvironmental changes. Quaternary Geochronology 5, 360–364.

Thompson, L.G., Yao, T., Davis, M.E., Henderson, K.A., Mosley-Thompson, E., Lin, P.N., Beer, J., Synal, H.-A., Cole-Dai, J., Bolzan, J.F., 1997. Tropical climate instability: the last glacial cycle from a Qinghai-Tibetan ice core. Science 276, 1821–1825.

Tian, L., Yao, T., MacClune, K., White, J.W.C., Schilla, A., Vaughn, B., Vachon, R., Ichiyanagi, K., 2007. Stable isotopic variations in west China: a consideration of moisture sources. Journal of Geophysical Research 112, D10112. http://dx.doi.org/10.1029/2006JD007718.

Van Campo, E., Gasse, F., 1993. Pollen- and diatom-inferred climatic and hydrological changes in Sumxi Co basin (western Tibet) since 13,000 yr B.P. Quaternary Research 39, 300–313.

Van Der Woerd, J., Tapponnier, P., Ryerson, F.J., Meriaux, A.S., Meyer, B., Gaudemer, Y., Finkel, R.C., Caffee, M.W., Zhao, G.G., Xu, Z.Q., 2002. Uniform postglacial slip-rate along the central 600 km of the Kunlun Fault (Tibet), from ^{26}Al, ^{10}Be, and ^{14}C dating of riser offsets, and climatic origin of the regional morphology. Geophysical Journal International 148, 356–388.

Wünnemann, B., Demske, D., Tarasov, P., Kotlia, B.S., Reinhardt, C., Bloemendal, J., Diekmann, B., Hartmann, K., Krois, J., Riedel, F., Arya, N., 2010. Hydrological evolution during the last 15 kyr in the Tso Kar lake basin (Ladakh, India), derived from geomorphological, sedimentological and palynological records. Quaternary Science Reviews 29, 1138–1155.

https://doi.org/10.1016/j.yqres.2016.04.001 Published online by Cambridge University Press

Wünnemann, B., Yan, D.D., Ci, R., 2015. Morphodynamics and lake level variations at Paiku Co, southern Tibetan Plateau, China. Geomorphology 246, 489–501.
Yi, M., Barton, L., Morgan, C., Liu, D., Chen, F., Zhang, Y., Pei, S., Ying, G., Wang, H., Gao, X., Bettinger, R.L., 2013. Microblade technology and the rise of serial specialists in north-central China. Journal of Anthropological Archaeology 32, 212–223.
Yu, G., Tang, L., Yang, X., Ke, X., 2001. Modern pollen samples from alpine vegetation on the Tibetan Plateau. Global Ecology and Biogeography 10, 503–519.
Zhang, D.D., Li, S.H., 2002. Optical dating of Tibetan human hand- and footprints: an implication for the palaeoenvironment of the last glaciation of the Tibetan Plateau. Geophysical Research Letters 29, 1072. http://dx.doi.org/10.1029/2001GL013749.

https://doi.org/10.1016/j.yqres.2016.04.001 Published online by Cambridge University Press